STUDY OF MINERAL STABILITY

IN THE

LUNAR ENVIRONMENT

BSR 1139

May 1965

Second Quarterly Progress Report

BSD Project No. 82911

Contract No. NAS 9-3734

for

NASA Manned Spacecraft Center

General Research Procurement Branch

2101 Webster - Seabrook Road

Houston, Texas 77058

BENDIX SYSTEMS DIVISION
OF
THE BENDIX CORPORATION
Ann Arbor, Michigan 48107

CONTENTS

CONTENTS (CONT.)

ILLUSTRATIONS

ILLUSTRATIONS (CONT.)

ILLUSTRATIONS (CONT.)

TABLES

SECTION 1

INTRODUCTION

This is the second quarterly report on Project NAS 9-3734, "Study of Mineral Stability in the Lunar Environment". The project was initiated on 16 November 1964; this report covers the period from 16 February 1965 to 16 May 1965.

The work has closely followed the program outlined in Bendix Systems Division's Technical Proposal BSD 965, August 1964, as supplemented by Bendix Letter 64-520-13913, 30 September 1964. Efforts during the three-month period covered in this report have been devoted to:

1. Completion of the synthesis of ammonium feldspar and the irradiation of a plagioclase
2. Completion of mass spectrometer analyses
3. Correlation of mass spectrometer analyses with DTA and TGA
4. Microscopic analyses of thin sections
5. Analysis of X-ray diffraction patterns taken at room temperature and pressure
6. Completion of special X-ray camera construction.

SECTION 2

TEST MINERALS

2.1 SYNTHESIS OF AMMONIUM FELDSPAR

The synthesis of a small amount (0.1 gm) of ammonium feldspar was described in the previous quarterly report. In the second quarter, Bendix attempted to synthesize 150 gm of ammonium feldspar in one batch. To produce this amount, larger copper capsules and a larger pressure vessel has to be used to contain the reactants. Problems immediately arose because of the difficulty of sealing the bigger tubes and in maintaining pressure in the larger reactor.

The attempt to seal 150 gm of anorthoclase together with an alkaline ammonium chloride solution into one large copper capsule, which was subsequently to be installed in a 500-ml steel reactor (Figure 2-1), was unsuccessful. Because an adequate seal could not be achieved, it was decided to seal about 50 gm of anorthoclase into two smaller tubes. These were inserted into the 500-ml reactor (together with enough water to provide the same pressure outside as inside the copper tubes) then placed inside a furnace and heated to 500°C. The reactor did not hold the pressure, and thus the solution inside the copper tubes leaked out.

Since the leaking of the solution did not seem appreciably to affect the steel of the 500-ml reactor, it was thought that perhaps the copper tubing, serving only to protect the steel, was unnecessary. The 100-ml reactor (Figure 2-2), used in the preliminary experiments, was made of different type of steel that corroded easily. The next step was to determine whether the 500-ml reactor would hold pressure under the required conditions. Several attempts were made without the aid of copper tubes, and these resulted in failure. It was concluded that the steels comprising the reactor would not allow a tight seal to be maintained at 500°C. The reactor was rated for use only to 350°C and 12,000 psi. Upon refinishing the sealing surfaces, it was possible to hold water at 350°C and 10,000 psi.

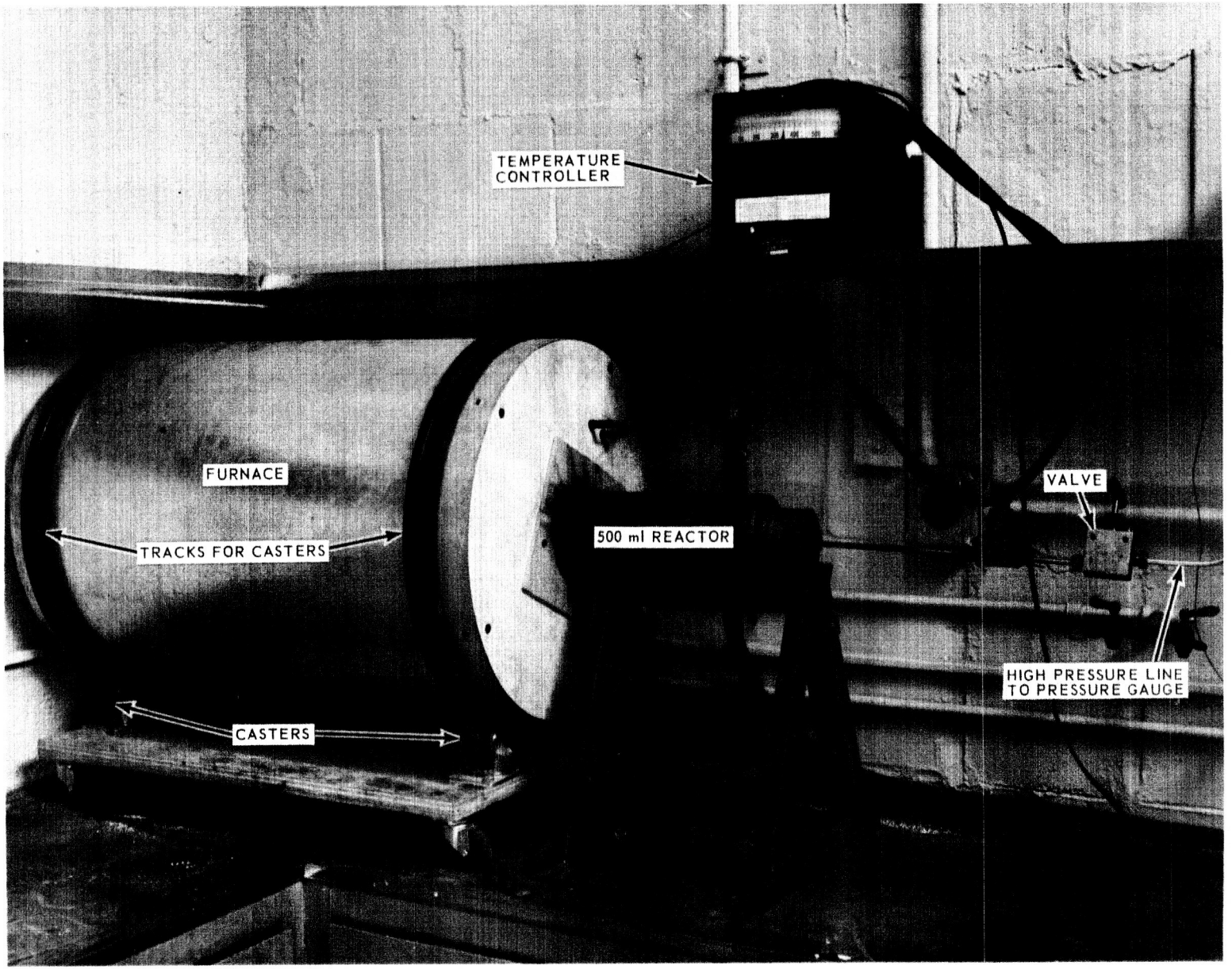

Figure 2-1 Experimental Apparatus Assembled and Ready to Be Placed in Furnace

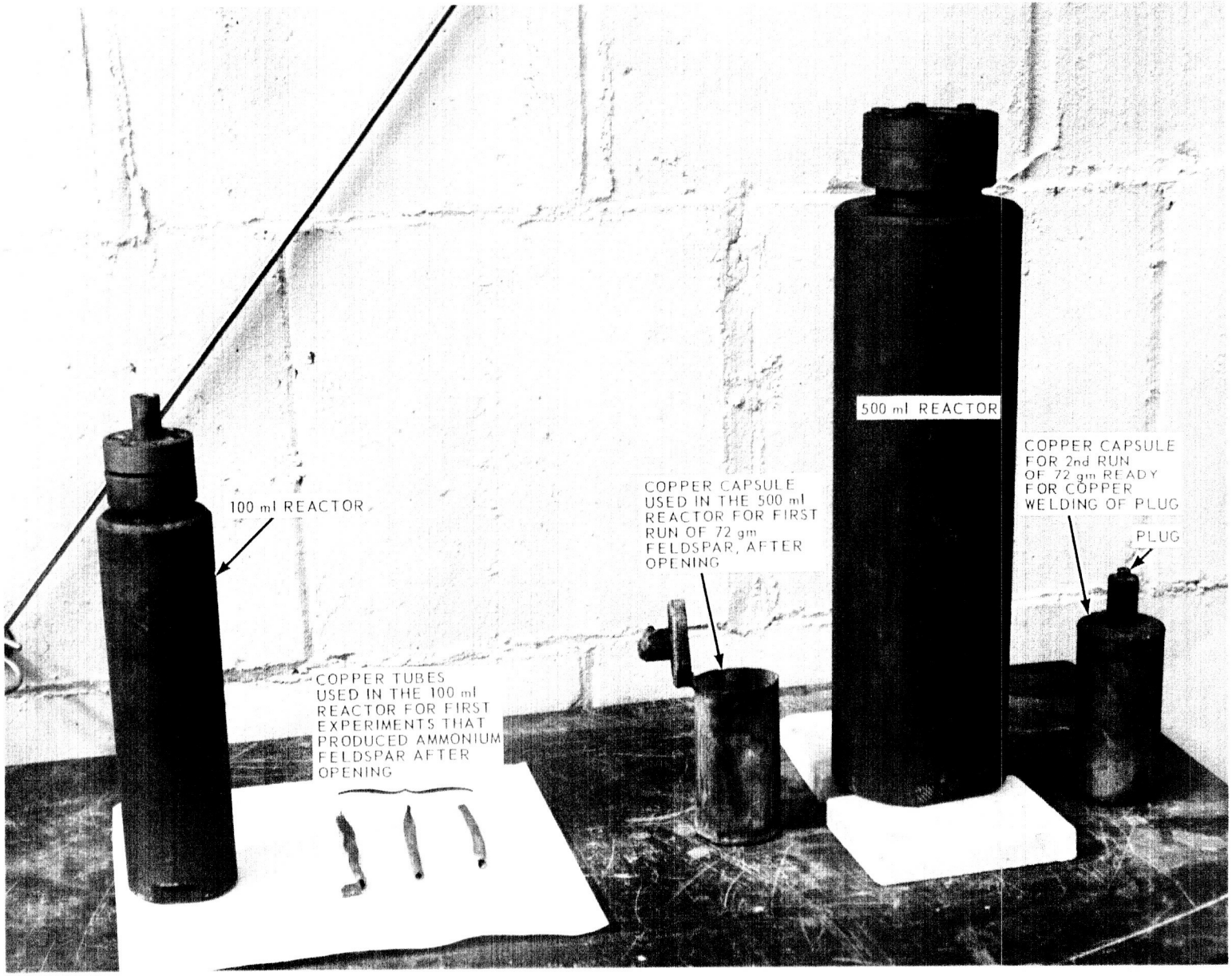

Figure 2-2 Reactors and Copper Capsules Used for Producing Ammonium Feldspar

Experiments were then performed to determine if the same solution, which produced ammonium feldspar in the 100-ml reactor at 500°C, would also do so at 350°C. After 48 hours in the 100-ml vessel, no reaction was detected. Subsequently, a stronger solution of 1 gm NH_4Cl, 2 ml H_2O, and enough NH_4OH to bring the pH to 8.5 did produce ammonium feldspar.

When the 500-ml reactor was loaded with the above solution, the vessel failed to hold the pressure. The reason for the leak is not clear. It might have been due to a small leak caused by rapid heating of the outside of the reactor that induced just enough expansion away from the cooler interior to open a minute hole. Once the leak started, the solution may have corroded the steel actively at two points resulting in deep etch pits. The leak could also have started from corrosion localized at the highest stress points on the sealing surface. The resulting corrosion necessitated extensive remachining and the fabrication of a new sealing ring.

To prevent the recurrence of this type of problem, a copper capsule was designed and copper welded at a local welding shop. This capsule was completely closed, except for a small hole left for filling with the anorthoclase and solution. A copper plug was inserted into the filling hole, after loading with 72 gm of anorthoclase plus a suitable amount of solution, and was then copper welded into the capsule. Thereafter, the capsule was placed inside the 500-ml reactor. Water was added to provide the pressure, and after sealing, the reactor was put into a furnace set for 350°C.

The reactor did not initially hold 10,000 psi for long periods, but pressure can be maintained reasonably well by occasionally pumping in more water. Later, the pressure remained constant at about 10,000 psi. Furthermore, the tubular furnace, into which the 500-ml reactor fits, has recently been fitted with encircling tracks and supported on casters to permit rotation of the furnace. It is expected that thorough mixing of the batch will facilitate the reaction of the anorthoclase with the solution. This treatment produced at the end of one week ammoniated products which are still under investigation.

2.2 REACTOR IRRADIATION OF PLAGIOCLASE

As described in the previous quarterly report, samples of finely pulverized labradorite (100, 200, and 300 mesh) have been irradiated in the Ford Nuclear Reactor, The University of Michigan, for 30 hr at the core

face. In response to our question concerning the hazard in working with this material after the short-lived (15 h) Na^{24} has decayed to an undetectable level (14 days cooling time), a sample of the irradiated plagioclase (22.3 mg) was counted in a windowless, gas flow proportional counter. With an assumed efficiency of 50%, the gross beta activity was calculated at 2.3×10^{-3} uc/mg.

The same sample was placed on a spectrometer and the only photopeaks that could be identified were from Fe^{59} (gamma energy 1.09 and 1.289 mev). The quantity of Fe^{59} was judged to be about 8.4×10^{-6} uc/mg. If it is assumed that all of the beta activity is due to Ca^{45} (T 1/2 = 160 d), then taking the specific activity to be 2.3×10^{-3} uc/mg, one must injest

$$\frac{30 \text{ uc}}{2.33 \times 10^{-3} \text{ uc/mg}} = 12.9 \times 10^{3} \text{ mg} = 12.9 \text{ gm}$$

in order to consume an amount equal to the maximum permissible body burden of 30 uc. As an aerosol, one would have to maintain a dust load of 1.2 mg/ft^3 to maintain the activity in the air at the maximum permissible concentration for insoluble Ca^{45}.

The problem is therefore reduced to one of using reasonable caution in opening the quartz tubes and in loading sample tubes. This work should be done in a dead air space, such as a glove box, to prevent the spread of troublesome contamination.

SECTION 3

X-RAY PHOTOGRAPHIC INVESTIGATION

3.1 PURPOSE OF AMBIENT X-RAY PATTERNS

Preliminary Debye-Scherrer photographs of all minerals to be examined subsequently under vacuum in the long-term experiment have been obtained at room temperature and pressure. These photographs were taken for two reasons:

1. To provide standard patterns as obtained under normal, familiar operating conditions. This is particularly important as regards several of the mineral phases, which, under natural conditions, show wide ranges in solid solution. Their powder photographs, therefore, are likely to exhibit significant variations from those published in the literature as standard patterns. These variations would undoubtedly be significant in reference to the possible changes brought about by structural or chemical transformations in the simulated lunar environment.

2. To confirm the identification of each test mineral. The X-ray data should substantiate the identifications by other methods, such as DTA and microscopic examination. The data would also provide information on the nature of contaminating phases, if any should occur. Furthermore, diffraction patterns confirm the compositional data in those phases which normally exhibit solid solution variations as a function of X-ray line position and relative intensity.

3.2 AMBIENT X-RAY PROCEDURES

All photographs were taken with a standard 57.3-mm-diameter Debye-Scherrer camera, using exposures of approximately three hours, except for the tektite and basalt glass specimens. The two exceptions were subjected to longer exposures for the possible detection of small amounts of crystalline phases.

All specimens were mounted in standard 0.2-mm-diameter glass capillaries. Several photographs were taken with FeK_α radiation to obtain better line resolution and to avoid fluorescence with iron-containing samples, while Cu K_α radiation was used with the others.

3.3 D-VALUES OF SAMPLE POWDER PATTERNS

The d-values measured from each photograph (by template) are listed in Table 3-1, along with the d-values obtained from the ASTM Powder Data file. A comparison of these values reveals that a 1:1 correspondence occurs between the experimental and ASTM values for the following specimens:

Actinolite (Figure 3-1)

Antigorite (Figure 3-2)

Ca-Montmorillonite (Figure 3-3)

Goethite (Figure 3-4)

Gypsum (var selenite) (Figure 3-5)

Hematite (Figure 3-6)

Muscovite (Figure 3-7)

Plagioclase (labradorite)-both irradiated (Figure 3-8) and non-irradiated (Figure 3-9)

Talc (Figure 3-10)

The actinolite pattern (Figure 3-1) showed a line with d = 4.2 Å that is not included in the ASTM standard list. However, this line does appear in the ASTM pattern for tremolite, of which actinolite is a variety having a slightly different composition. Thus, all lines are accounted for by actinolite alone.

The Tektite pattern (Figure 3-11) showed no lines at all, therefore confirming its non-crystalline nature. Likewise, basalt glass (Figure 3-12), except for one well-defined but weak line with its d-value equal to 2.5 Å, corresponds to a strong plagioclase line. This confirms the results of a previous optical examination, which disclosed the presence of a small amount of unfused plagioclase. One may reason, however, that since the photograph had been subjected to a longer exposure time, and since the line was weak, only a very small amount of plagioclase was present. Two other very weak lines were discernible with difficulty, but they too correspond to plagioclase lines.

TABLE 3-1

A COMPARISON OF EXPERIMENTAL AND ASTM D-VALUES, Å

ACTINOLITE

EXP (Å)	ASTM (Å)	EXP (Å)	ASTM (Å)		EXP (Å)	ASTM (Å)	EXP (Å)	ASTM (Å)
9.0	9.06	3.23	3.27		2.15	2.16	1.29	1.29
8.4	8.42	3.10	3.11		2.02	2.04	1.195	
5.1	5.12	2.93	2.94	Only dense lines	2.00	2.01	1.160	
4.8	4.88	2.70	2.71		1.67	1.65	1.080	End of List
4.5	4.52	2.58	2.59		1.57	1.58	1.070	
4.2	4.20 (Tremolite)	2.52	2.53		1.50	----	1.045	
3.82	3.81	2.32	2.33		1.43	1.43	1.027	
3.38	3.38	2.25	2.27		1.36	----	0.982	

AMMONIUM FELDSPAR

(Sample Not Available)

ANTIGORITE

7.2	7.28	2.79	2.798	2.15	2.15	1.49	1.49
4.6	4.64	2.50	2.51	2.09	2.12	1.31	1.315
3.83	3.91	2.45	2.45	1.53	1.53		

BASALT GLASS

3.1	----	2.5	2.51 (Plagioclase)	2.3	----		

CALCITE

3.8	3.86	1.86	1.875	1.33	1.339	1.06	1.0613
3.3	3.4 (Aragonite)	1.60	1.604	1.29	1.297	1.04	1.0473
3.0	3.035	1.52	1.525	1.24	1.247	1.03	1.0352
2.49	2.495	1.47	1.473	1.23	1.235	1.01	1.0118
2.28	2.285	1.44	1.440	1.18	1.179	0.98	0.9846
2.08	2.095	1.41	1.422	1.15	1.1538	0.96	0.9655
1.90	1.913	1.36	1.356	1.14	1.1425		

Ca-MONTOMORILLONITE

Diffuse Lines 4.50	4.50	3.10	3.02	1.69	1.70	1.29	1.285
Diffuse Lines 4.05	4.05 (Kerr (1936))	2.55	2.58, 2.50	1.49	1.49	1.24	1.24

GOETHITE

5.0	5.0	2.00	2.00	1.45	1.456	1.15	1.151
4.2	4.21	1.92	1.92	1.42	1.42	1.14	1.141
3.38	3.37	1.80	1.80	1.39	1.392	1.125	1.125
2.70	2.69	1.72	1.719	1.35	1.347	1.065	1.071
2.58	2.57	1.69	1.689	1.32	1.318	1.050	End of List
2.45	2.44	1.60	1.602	1.262	1.263	1.022	
2.25	2.25	1.56	1.563	1.242	1.239	1.01	
2.18	2.18	1.51	1.507	1.19	1.197	0.995	0.996

GYPSUM

7.5	7.56	2.67	2.679	1.77	1.778	1.32	1.32
4.3	4.27	2.49	2.495	1.66	1.664	1.24	1.25

3.01	3.06	2.08	2.08	1.58	1.584	1.13	
2.85	2.867 pair	1.87	1.879	1.44	1.439	1.08	End of List
2.75	2.786	1.80	1.796	1.36	1.365		
			HEMATITE				
3.7	3.66	1.84	1.838	1.45	1.45	1.16	1.162
2.7	2.69	1.69	1.69	1.35	1.349	1.14	1.141
2.57	2.57	1.59	1.59	1.26	1.258	1.10	1.10
2.20	2.201	1.49	1.484	1.19	1.189	1.055	1.055
						1.039	1.038
			MUSCOVITE				
9.90	9.95	2.95	2.987	2.12	2.132	1.35	1.352
4.9	4.97	2.82	2.859	1.97	1.972	1.33	1.335
4.5	4.47	2.75	2.789	1.70	1.704	1.155	1.1582
3.95	3.95	2.57	2.566	1.65 pair	1.646	1.13	1.1300
3.85	3.882	2.45	2.450	1.60	1.603	1.100	1.167
3.50	3.489	2.38	2.384	1.55	1.559	1.065	----
3.30	3.32	2.25	2.254	1.50	1.504	1.047	---- End of List
3.20	3.199	2.20	2.208	1.44	1.453	----	----
			NATROLITE				
6.5	6.6	2.57	2.57	1.75	1.75	1.33	1.33
6.0	5.9	2.45	2.43	1.72	1.72	1.30	1.31
4.1	4.13	2.33	2.32	1.62	1.62	1.23	1.24
4.4	4.38	2.25	2.26	1.57	1.53	1.21	1.22
4.7	4.63	2.19	2.18	1.54	1.52 (Scolecite)	1.19	1.19
3.55	3.63 (Scolecite)	2.05	2.05	1.47	1.46	1.14	1.14
3.2	3.16	1.95	1.95	1.44	1.43 (Scolecite)	1.09	1.08
2.95	2.94	1.87	1.87	1.42	1.42	1.06	1.06
2.85	2.86	1.80	1.80	1.38	1.38	1.02	1.02
2.65	2.68						
			PLAGIOCLASE				
			(Irradiated And Non-Irradiated)				
6.5	6.48	2.50	2.51	1.77	1.77	1.34	1.35
4.0	4.04	2.29	2.29	1.60	1.62	1.26	1.27
3.7	3.75	2.10	2.12	1.57	1.56	1.24	1.25
3.2	3.20	2.00	2.01	1.54	1.53	1.21	1.21
2.9	2.95	1.91	1.92	1.49	1.48	1.15	1.16
2.8	2.84	1.82	1.83	1.38	1.37	1.13	1.13
2.65	2.66						
			TALC				
9.3	9.34	2.45	2.476	1.72	1.725	1.33	1.336
4.7	4.66	2.2	2.212	1.67	1.682	1.31	1.318
3.1	3.116	2.08	2.10	1.52	1.527	1.29	1.297
2.6	2.629	1.85	1.870	1.39	1.394	1.27	1.269

TEKTITE

No lines were observed on the film.

The calcite x-ray pattern (Figure 3-13) showed one very weak line (d = 3.3 Å) that is not associated with calcite. This line corresponds to the strongest line of aragonite, a high-pressure polymorph of calcite. It is well known that calcite can be transformed into aragonite with grinding. Consequently, it is not surprising that we find a very small amount of aragonite present in the sample (< 1%.) Heating the sample should cause the aragonite to retransform into calcite. Mention should be made of the very small but broad exothermic peak noted at 250°C on the DTA curve of calcite. This probably corresponds to the inversion.

The natrolite pattern (Figure 3-14) showed contamination by a second phase. Most lines were readily indexable with natrolite d-values, but some still remained. Although zeolites yield very complex powder patterns, with considerable overlap occurring between lines of different phases, the remaining lines were readily indexable as belonging to scolecite. This confirms the optical examination of the specimen. However, the relative intensities of the natrolite and scolecite lines indicate that there is relatively little scolecite present.

After 30 hours of neutron exposure at the core face of The University of Michigan nuclear reactor, no detectable difference was noted between the pattern of the irradiated plagioclase (Figure 3-7) and that of the non-irradiated plagioclase (Figure 3-8).

In summary, it appears that all specimens are sufficiently pure for the purpose of this experiment, at least insofar as the evidence from the X-ray examination is concerned. Standard photographs of each phase will also be obtained in the vacuum chamber at regular intervals throughout the long term experiment.

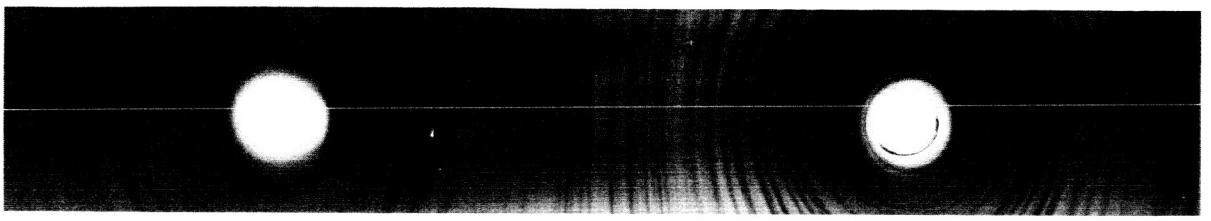

Figure 3-1 Actinolite X-Ray Pattern

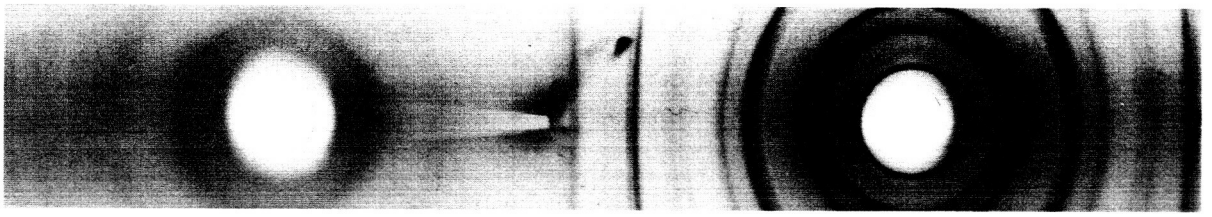

Figure 3-2 Antigorite X-Ray Pattern

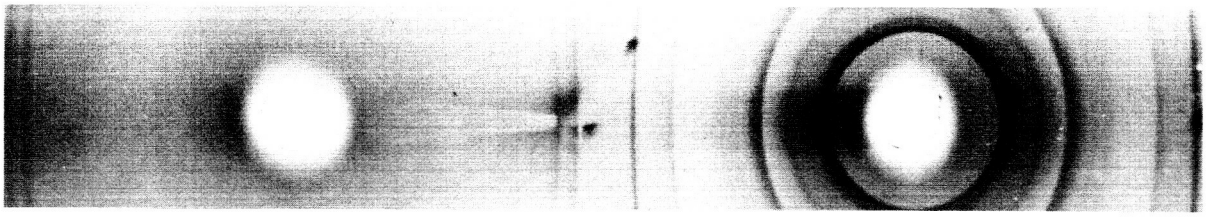

Figure 3-3 Ca-Montmorillonite X-Ray Pattern

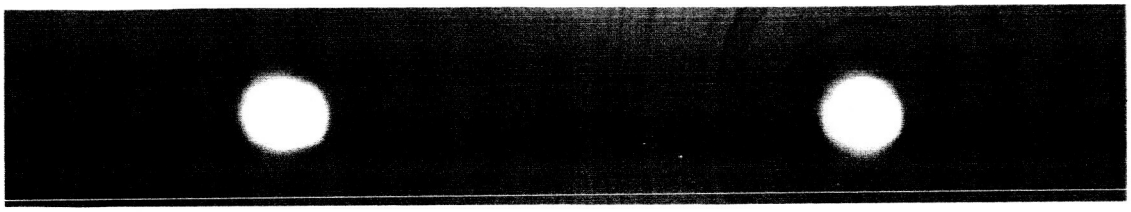

Figure 3-4 Goethite X-Ray Pattern

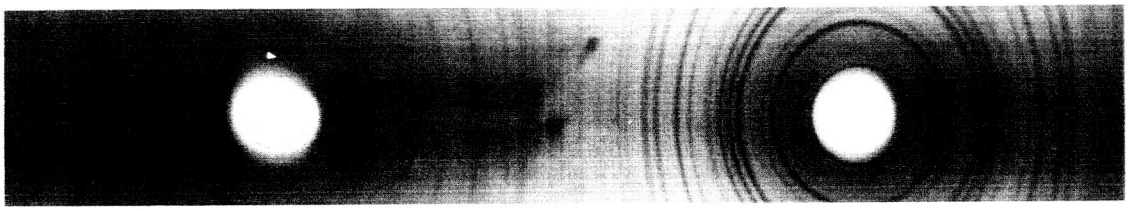

Figure 3-5 Gypsum X-Ray Pattern

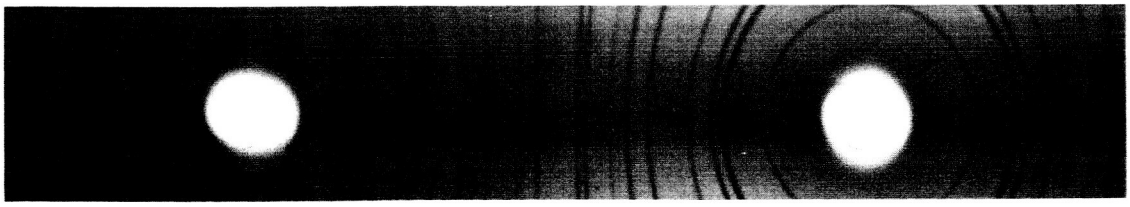

Figure 3-6 Hematite X-Ray Pattern

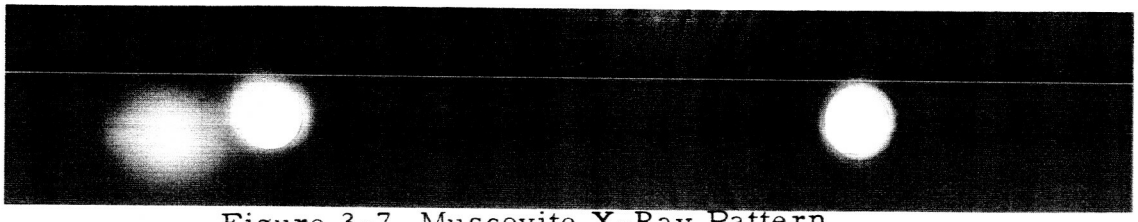

Figure 3-7 Muscovite X-Ray Pattern

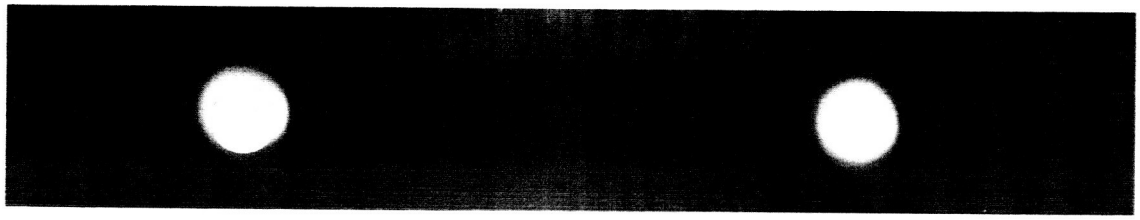

Figure 3-8 Plagioclase (Irradiated) X-Ray Pattern

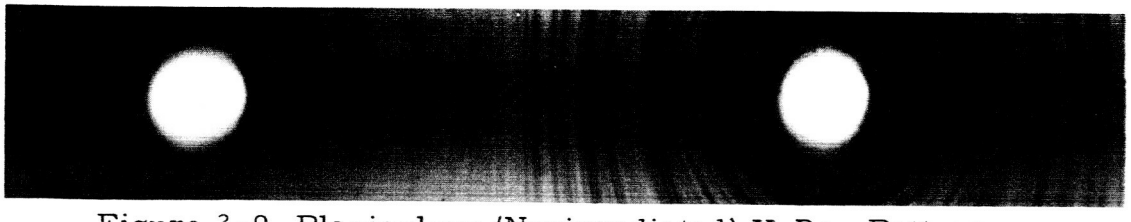

Figure 3-9 Plagioclase (Nonirradiated) X-Ray Pattern

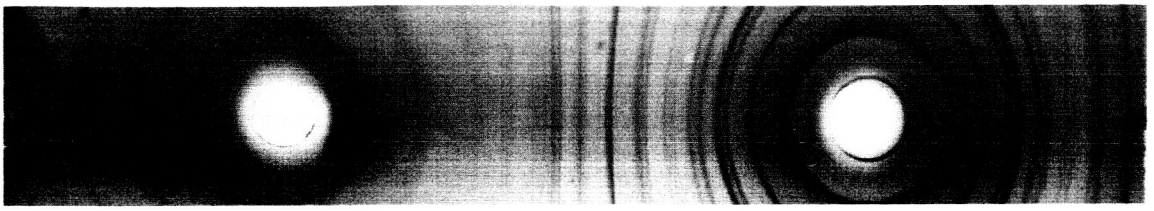

Figure 3-10 Talc X-Ray Pattern

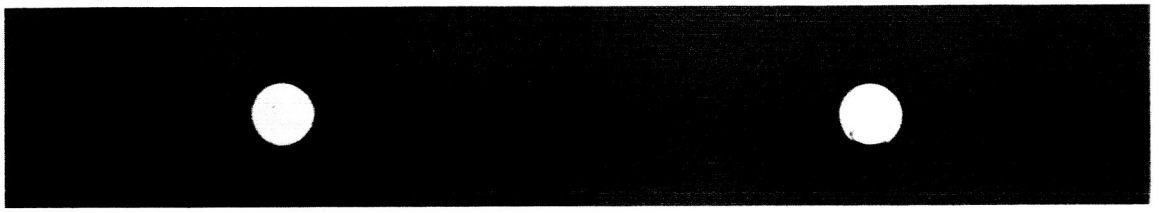

Figure 3-11 Tektite X-Ray Pattern

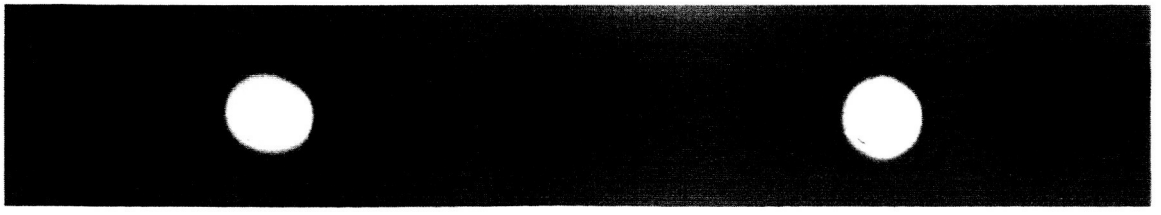

Figure 3-12 Basalt Glass X-Ray Pattern

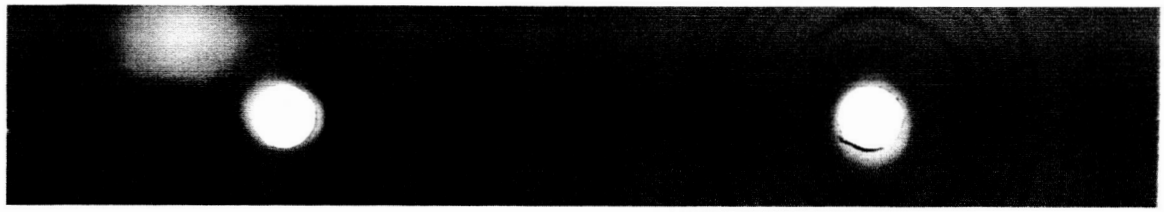

Figure 3-13 Calcite X-Ray Pattern

Figure 3-14 Natrolite X-Ray Pattern

SECTION 4

MASS SPECTROMETER INVESTIGATION

The mass spectrometer analyses of six of the 14 test minerals were presented in the proceding quarterly report without comparison to their DTA and TGA curves. Having completed the mass spectrometer analyses of the remaining specimens during the second quarter, Bendix must correlate the results of all 14 test minerals with their previously reported DTA and TGA curves. For the sake of completeness, the mass spectrometer curves that appeared in the first progress report have also been included in this report.

4.1 ACTINOLITE

The mass spectrometer curve (Figure 4-1) shows a small absorbed* water loss. The two peaks in the curve, at 430°C and 790°C, represent the loss of hydroxyl ion. These peaks correspond to endothermic peaks at 610°C and 1035°C on the DTA curve. The 430°C peak is probably due to the loss of OH^- from chlorite, a possible impurity in the sample. The other peak corresponding to 790°C on the mass spectrometer curve and 1035°C on the DTA curve is definitely attributed to the loss of OH^- from the actinolite.

4.2 AMMONIUM FELDSPAR

The mass spectrometer analysis was run on the "pilot" batch of NH_4 feldspar. Because of the minute amount of sample produced, the available material was sufficient for only the mass spectrometer analysis. The three curves included in Figure 4-2 represent the H_2O, NH_3, and NH_2. The H_2O curve describes the combined loss of zeolitic water and water resulting from the complete structural breakdown. Vaporization of zeolitic water occurs at 30°C. The NH_3 and associated structural water are lost at 52°C, and the appearance of NH_2 is due to the decomposition of NH_3 induced by the electron beam.

*The term "absorbed water" is used in this report to include water taken from the atmosphere in any manner whatever, whether by physical adsorption, formation of a hydrate, or in some other way.

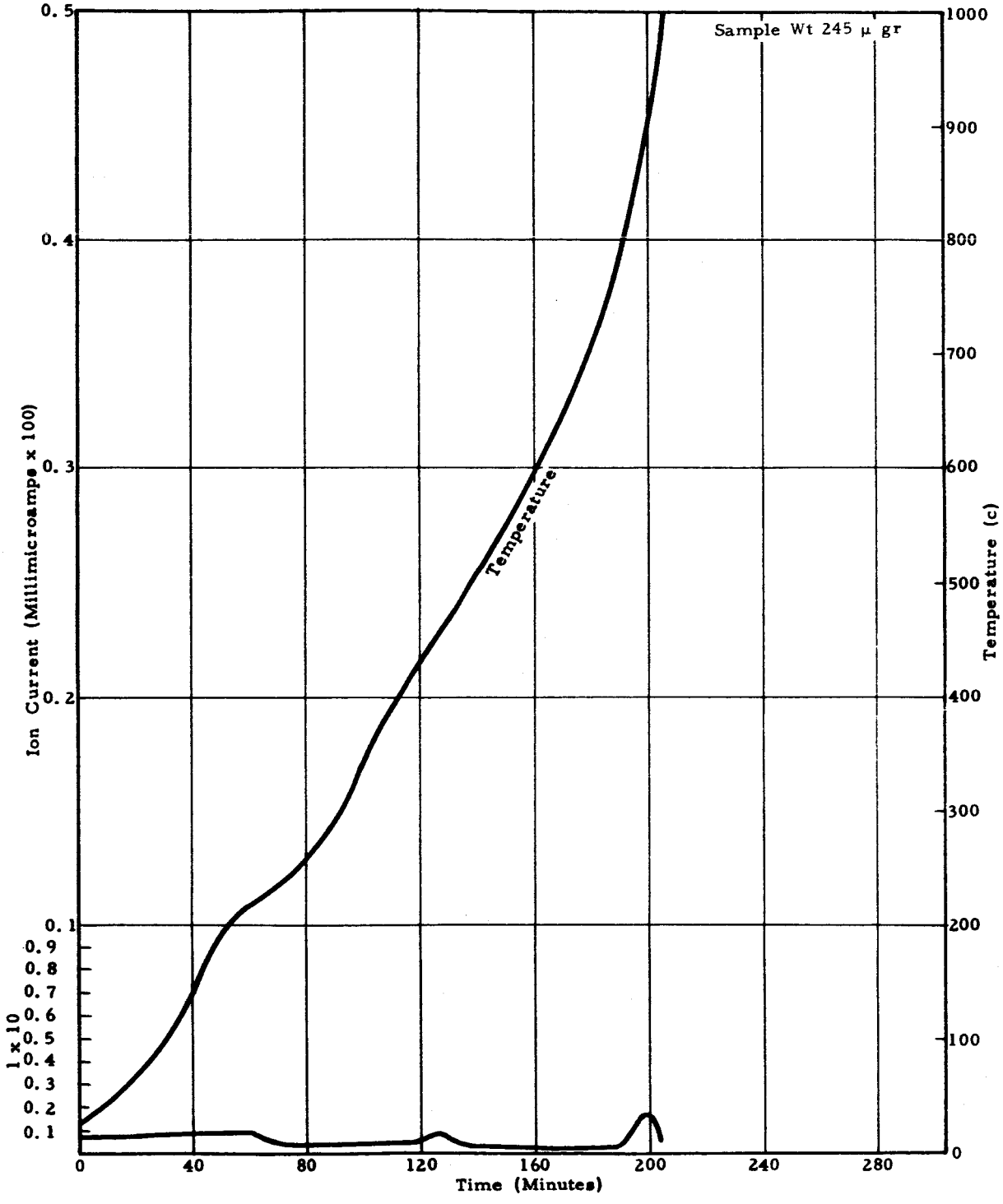

Figure 4-1 Mass Spectrometer Analysis of Actinolite—Scan With H_2O Peak Plotted

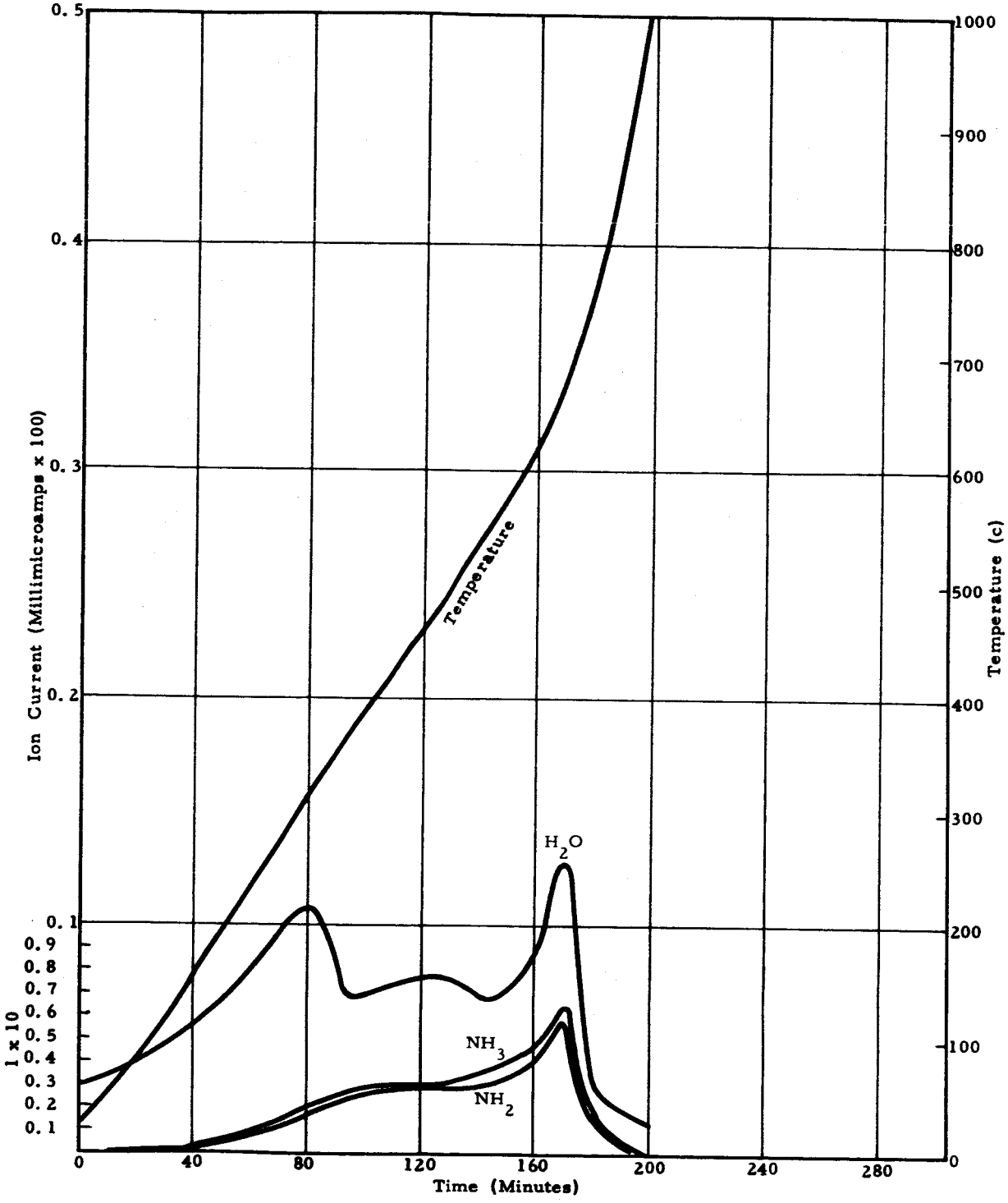

Figure 4-2 Mass Spectr ›meter Analysis of Ammonium Feldspar—H_2O NH_2, and NH_3 Peaks Plotted

4.3 ANTIGORITE

The antigorite sample begins to decompose at 270°C, under the vacuum conditions prevailing in the mass spectrometer. The loss of OH^- produces a curve (Figure 4-3) consisting mainly of two large, closely spaced peaks. This reaction is represented on the DTA curve by a peak at 710°C and minor shoulder at 670°C. The phase transition, indicated by a sharp endothermic peak at 822°C on the DTA, is not detectable in the mass spectrometer.

4.4 BASALT GLASS

A very small loss of absorbed water, (< 1%) is evident in the mass spectrometer curve (Figure 4-4). In contrast, the DTA curve is quite complex, showing exothermic peaks at 640°C, 738°C, 853°C, 977°C, and an endothermic peak at 1055°C. No reaction is noted in the mass spectrometer that might correspond to these peaks. Moreover, the TGA sample gained weight during the course of the experiment while the mass spectrometer sample did not. The gain in weight, as previously reported, could be the result of Fe oxidation. Because oxygen is absent in the mass spectrometer this would account for the absence of weight gain in the mass spectrometer sample.

4.5 CALCITE

The decomposition of calcite required several mass spectrometer curves (Figures 4-5 to 4-8) to monitor the volatiles. However, only one of the volatiles is the direct product of decomposition; viz., CO_2. The others result from the disruptive effects of the electron beam on the CO_2. Thus, the temperatures at which CO, C, and O appear closely approximate the temperature when the decomposition product, CO_2, appears. The mass spectrometer curve for the decomposition of calcite (Figure 4-5) reveals a large peak starting at 323°C. This corresponds to the large endothermic peak at 938°C on the DTA curve. The loss of absorbed water (Figure 4-6) is small, but is responsible for the slight endothermic drift in the DTA curve and the minute weight loss in the TGA curve. The amount of absorbed water lost is estimated at < 1%. The production of C and O is indicated in Figures 4-7 and 4-8.

4.6 CA—MONTMORILLONITE

The presence of impurities in the sample, such as illite, has complicated the mass spectrometer curve (Figure 4-9). It is extremely difficult

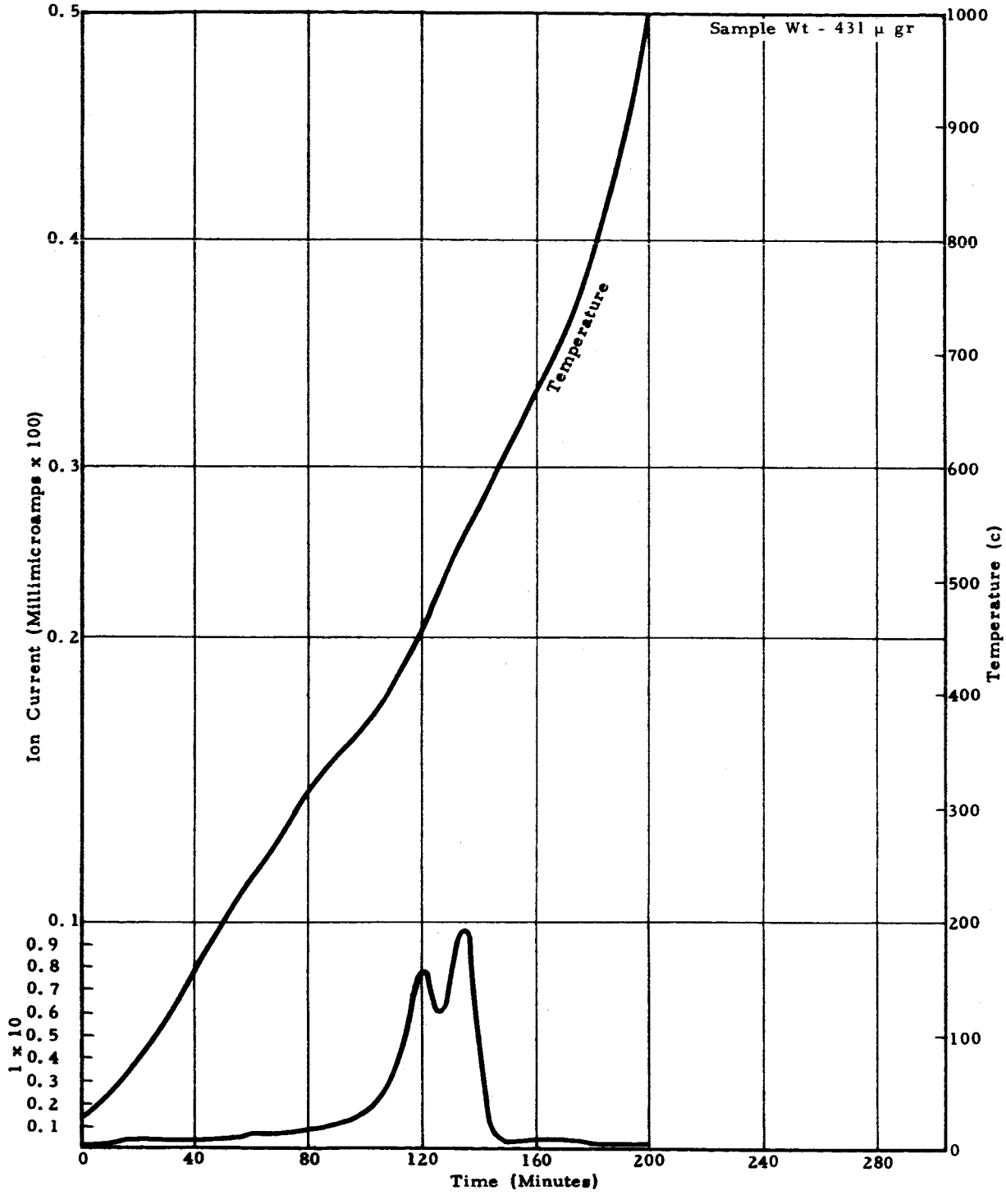

Figure 4-3 Mass Spectrometer Analysis of Antigorite—Scan With H_2O Peak Plotted

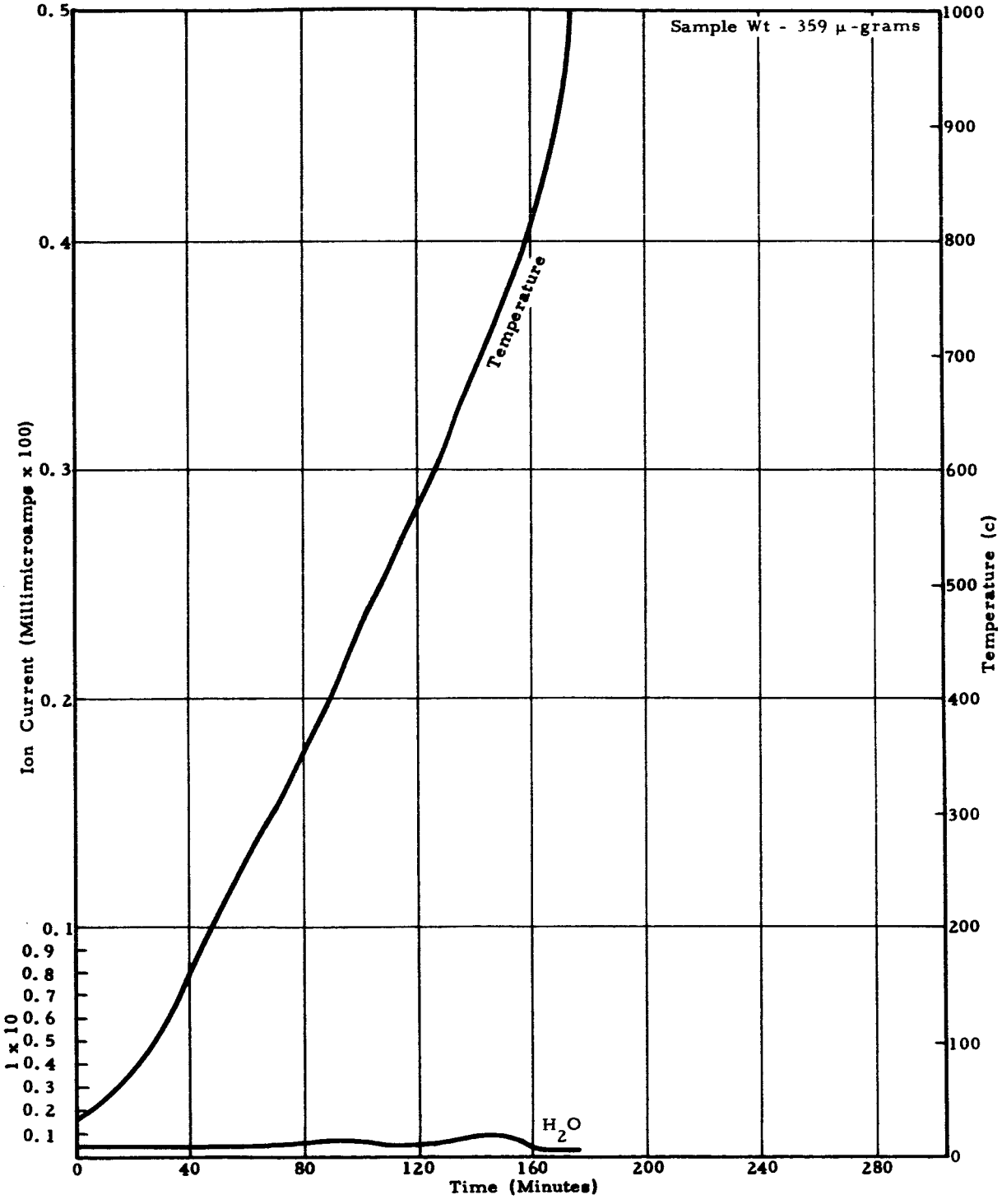

Figure 4-4 Mass Spectrometer Analysis of Basalt Glass—Scan With H_2O Peak Plotted

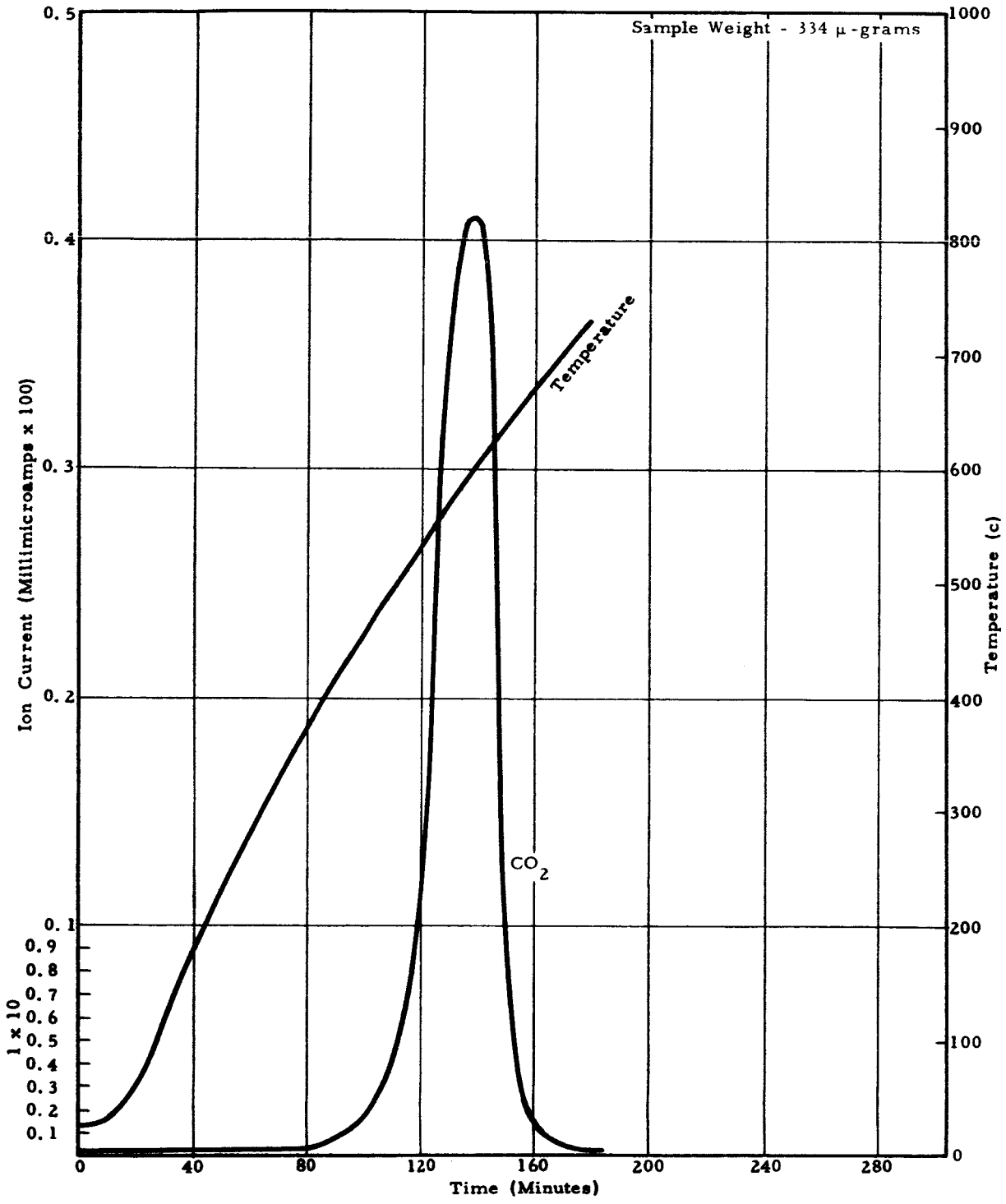

Figure 4-5 Mass Spectrometer Analysis of Calcite—Scan With CO_2 Peak Plotted

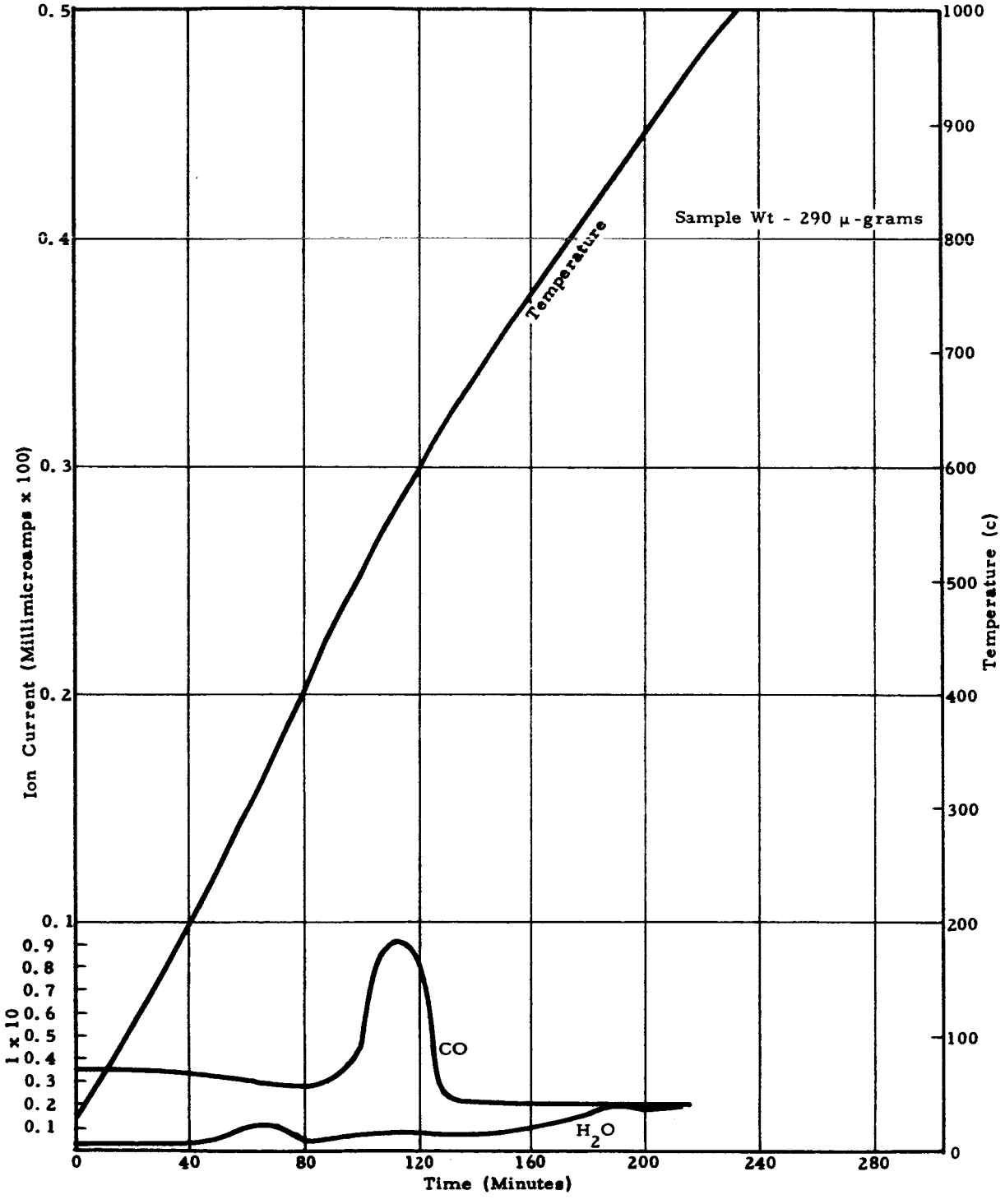

Figure 4-6 Mass Spectrometer Analysis of Calcite—CO and H_2O Peaks

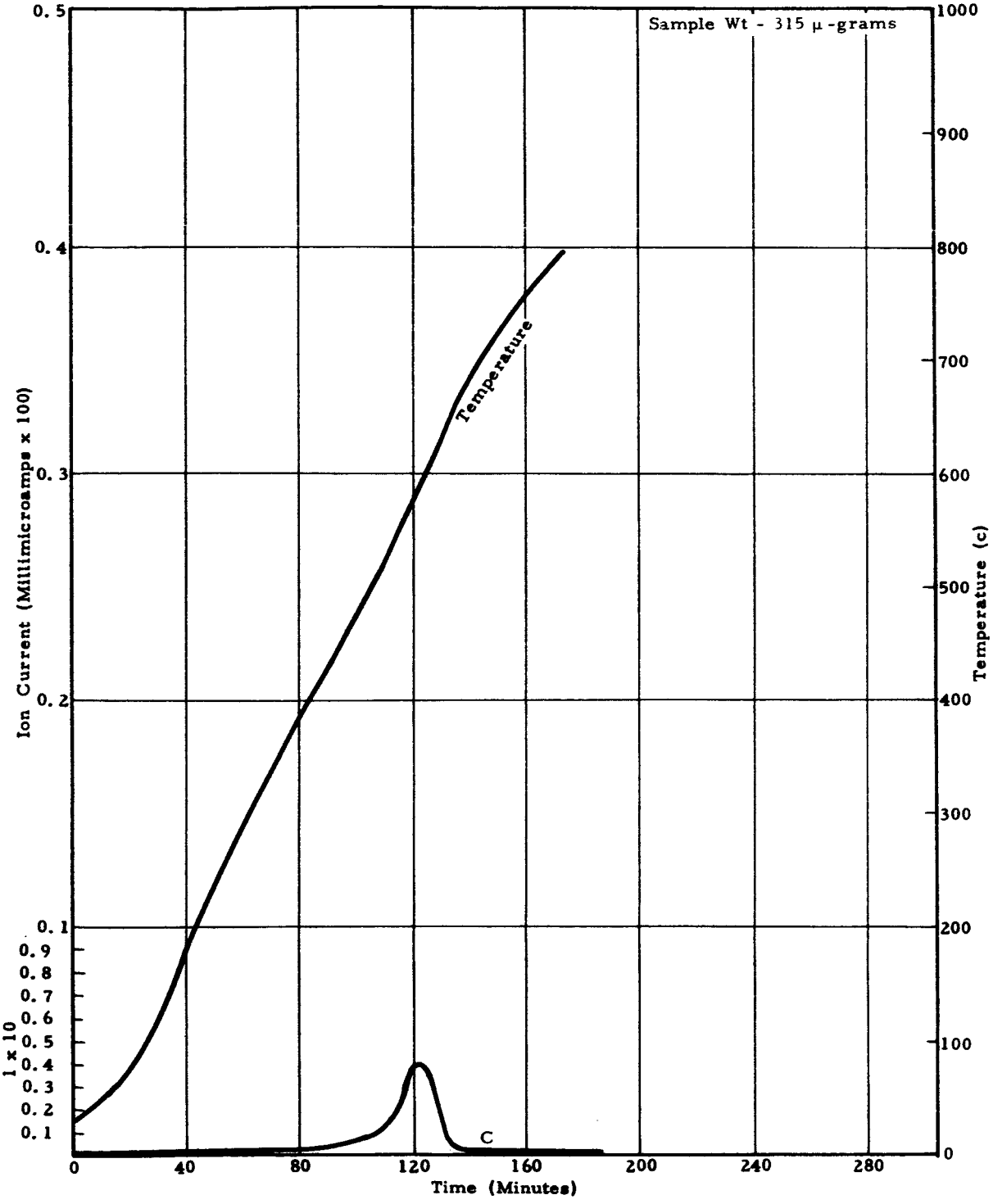

Figure 4-7 Mass Spectrometer Analysis of Calcite—C Peak

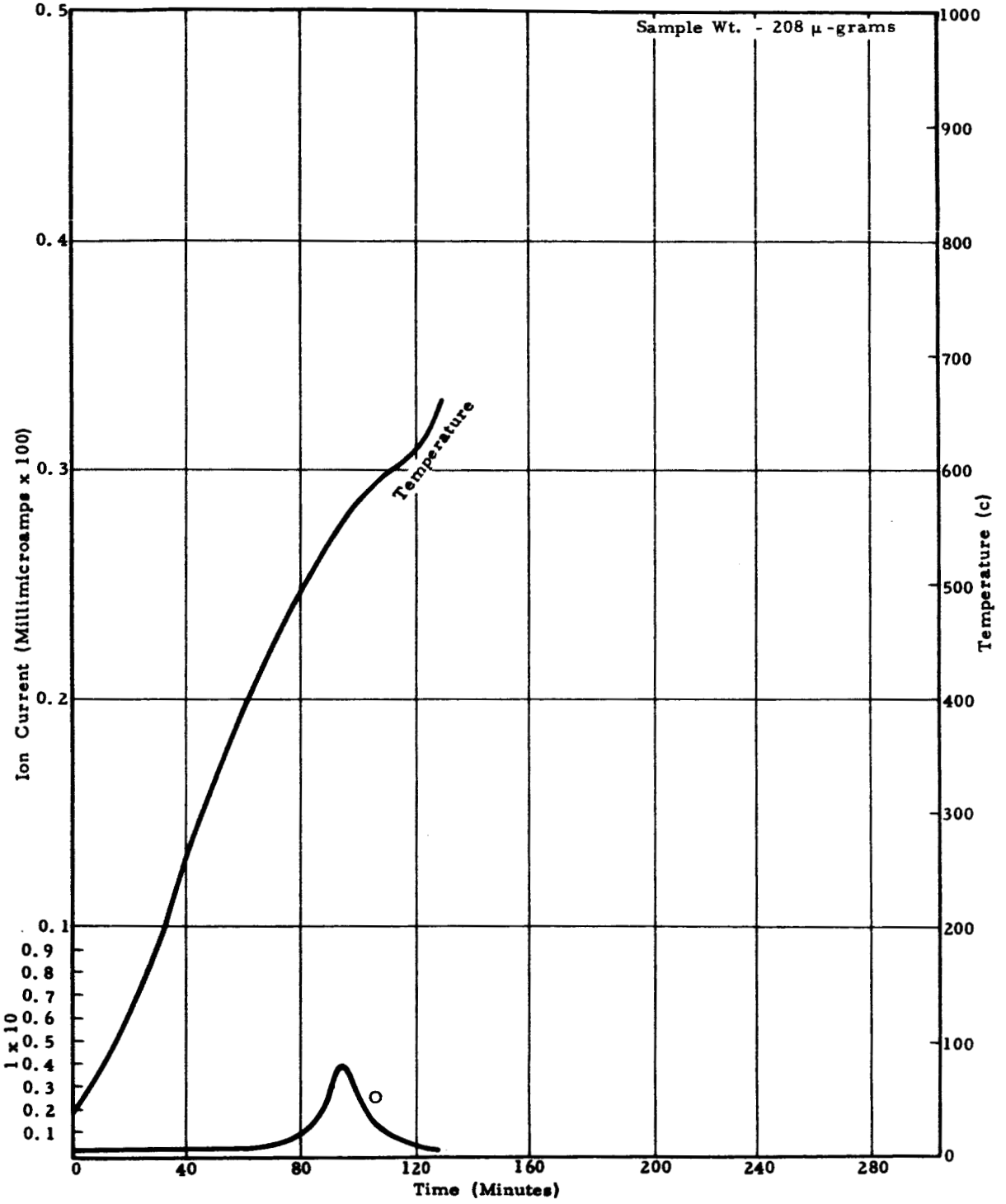

Figure 4-8 Mass Spectrometer Analysis of Calcite—O Peak

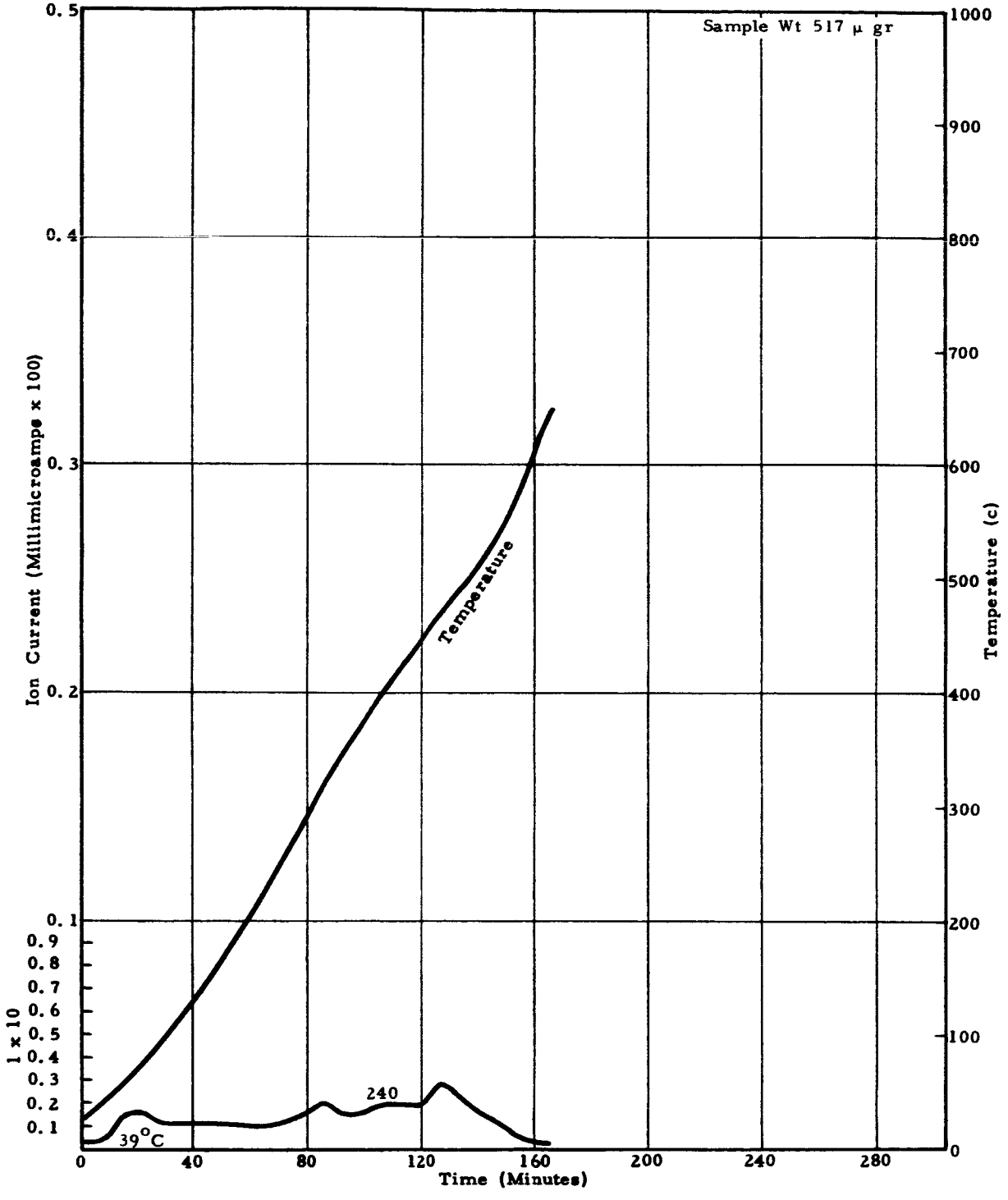

Figure 4-9 Mass Spectrometer Analysis of Ca-Montmorillonite—H_2O Peak

to determine precisely the temperature at which the OH^- volatilized. The increase of the water level at 39°C is attributed to the loss of water from illite, while the increase at 240°C is probably due to OH^- loss by the calcium montomorillonite. It is apparent from the size of the peaks that all of the interlayer water had been lost in vacuum. For comparison, the DTA curve shows peaks at 141°C and 202°C (corresponding to the interlayer water loss), a peak at 531°C (corresponding to the loss of OH^- by the illite), and a peak at 691°C (corresponding to the loss of OH^- by the montomorillonite.)

4.7 GOETHITE

This specimen decomposes at 44°C in the mass spectrometer (Figure 4-10). In contrast, the DTA curve shows a strong endothermic drift culminating in a sharp endothermic peak at 377°C. This drift is probably caused by the loss of absorbed water. The loss of absorbed water could not be detected in the mass spectrometer because of the low temperature at which the loss of OH^- occurred.

4.8 GYPSUM

The partial decomposition of gypsum (selenite) to the hemihydrate could not be observed in the mass spectrometer (Figures 4-11 and 4-12). This is explained by the fact that when gypsum is exposed to a pressure of 5×10^{-6} torr, it decomposes at a temperature of less than 27°C. It was evident by the high initial water level of the mass spectrometer curves. The transformation to anhydrous calcium sulfate began at 52°C, corresponding to the inflection points in the first two curves of Figure 4-12. In comparison, the DTA curves include two endothermic peaks, at 168°C and 203°C, corresponding to the formation of the hemihydrate and soluble $CaSO_4$. A third exothermic peak corresponds to the recrystallization of soluble $CaSO_4$ to anhydrite. This process was not evident in the mass spectrometer.

4.9 HEMATITE

A loss of absorbed water is indicated by the mass spectrometer curve (Figure 4-13) by the endothermic drift of the DTA curve, and by the weight loss shown by TGA curve. The amount of water loss is estimated at $< 1\%$ and may have originated from the water locked within the fibrous aggregate of the mineral. The small endothermic peak on the DTA curve at 350°C could not be related to a corresponding loss of volatiles in the mass spectrometer.

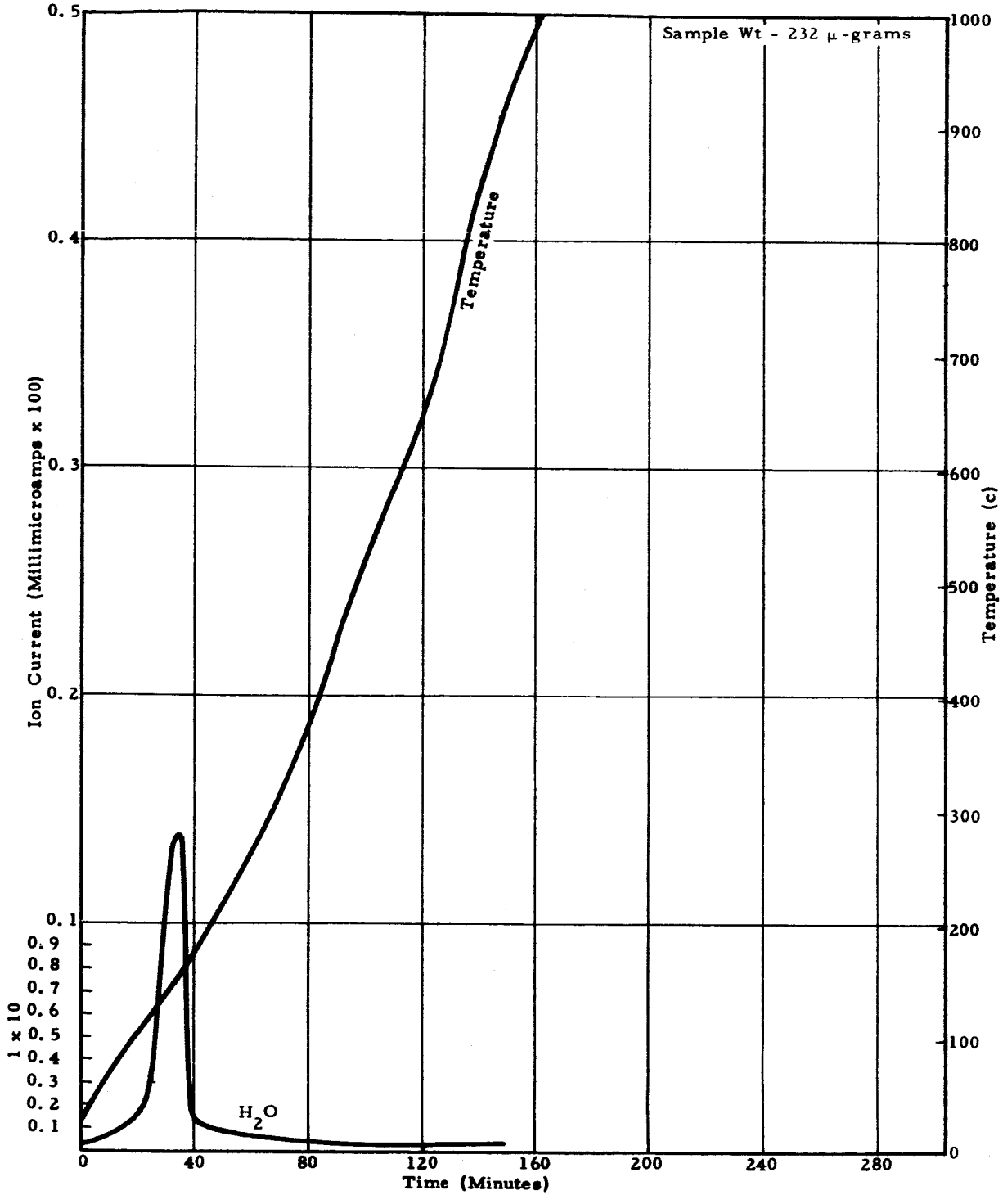

Figure 4-10 Mass Spectrometer Analysis of Goethite—Scan With H_2O Peak Plotted

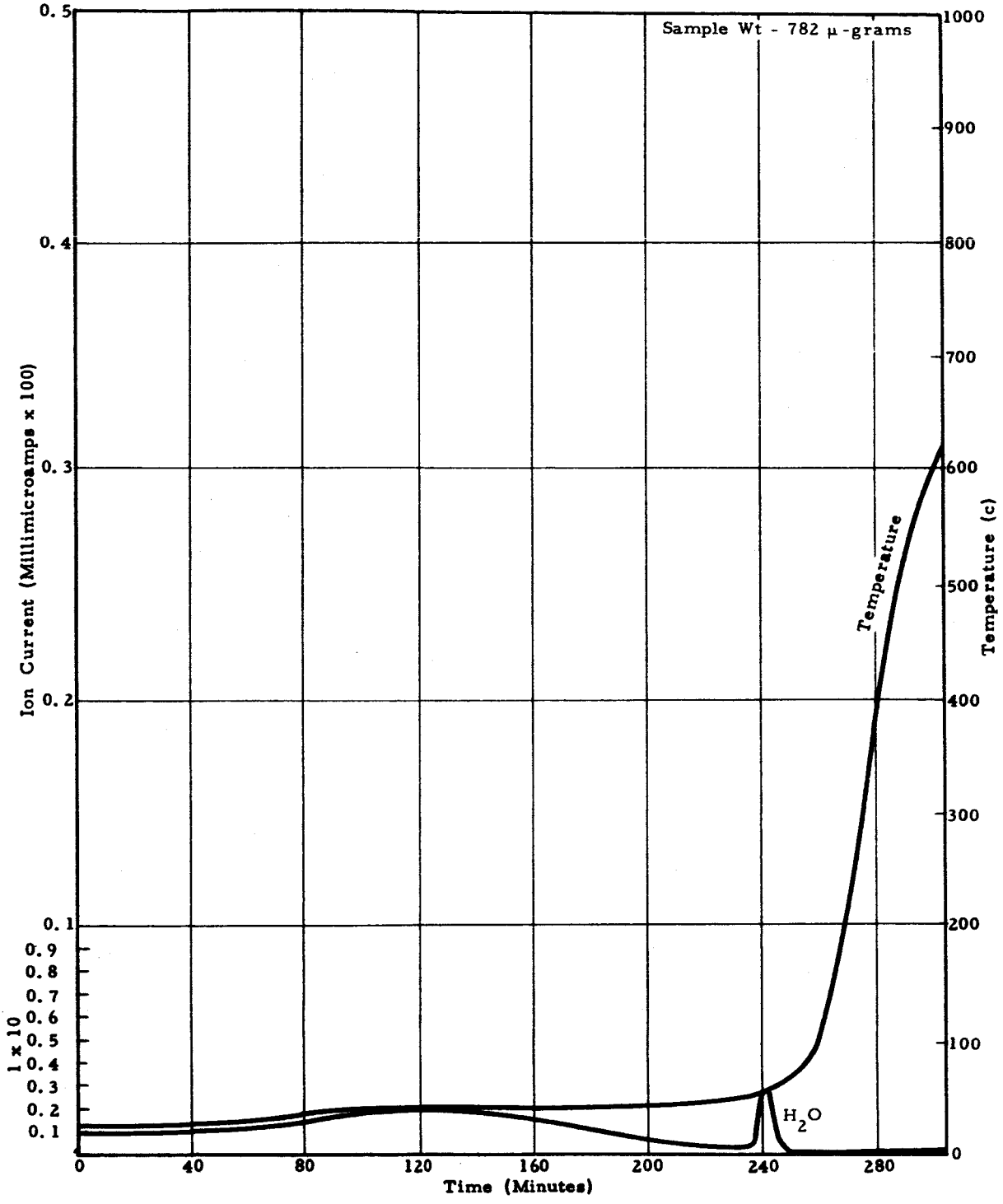

Figure 4-11 Mass Spectrometer Analysis of Gypum—H_2O Peak

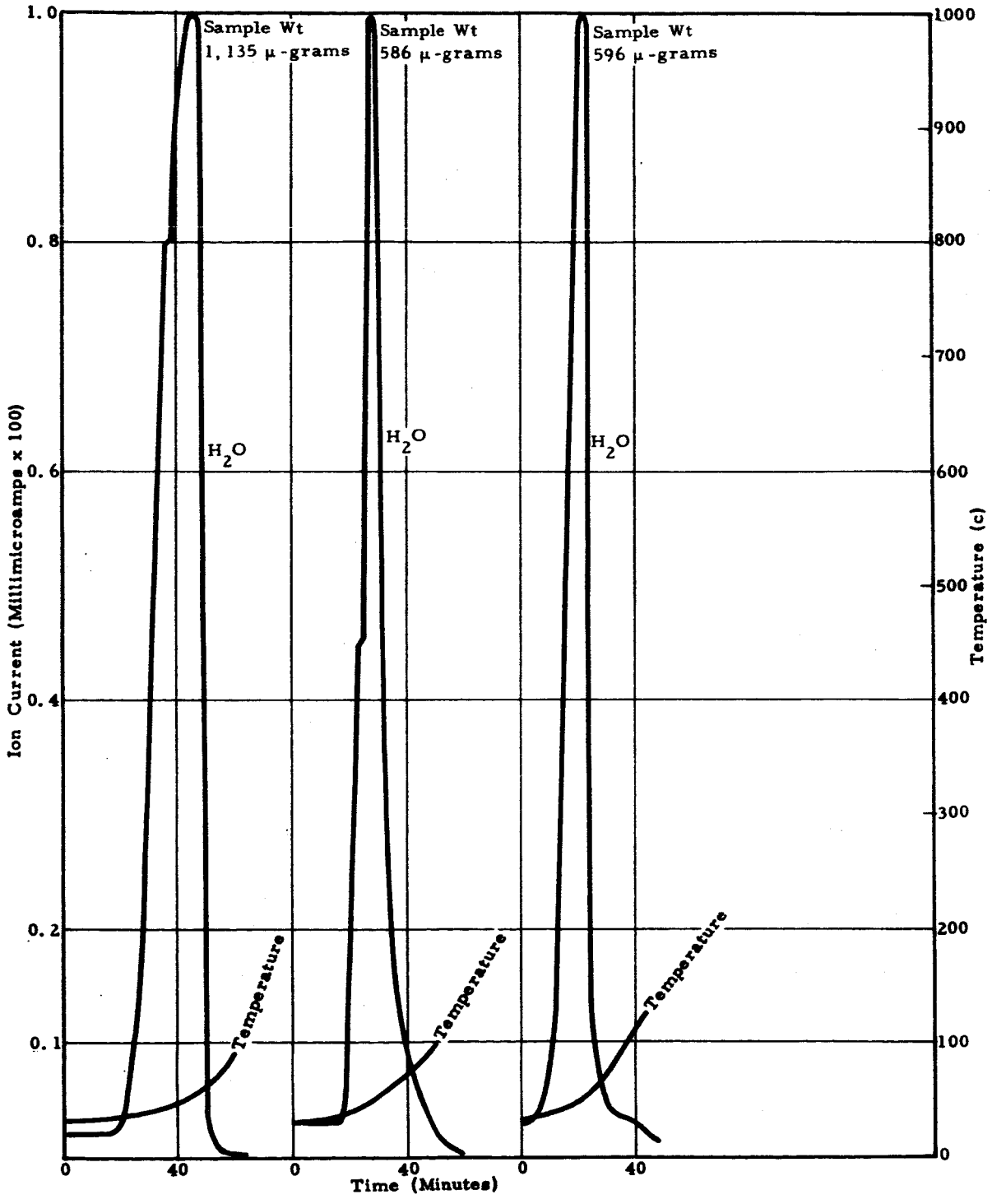

Figure 4-12 Mass Spectrometer Analysis of Gypsum–H_2O Peaks

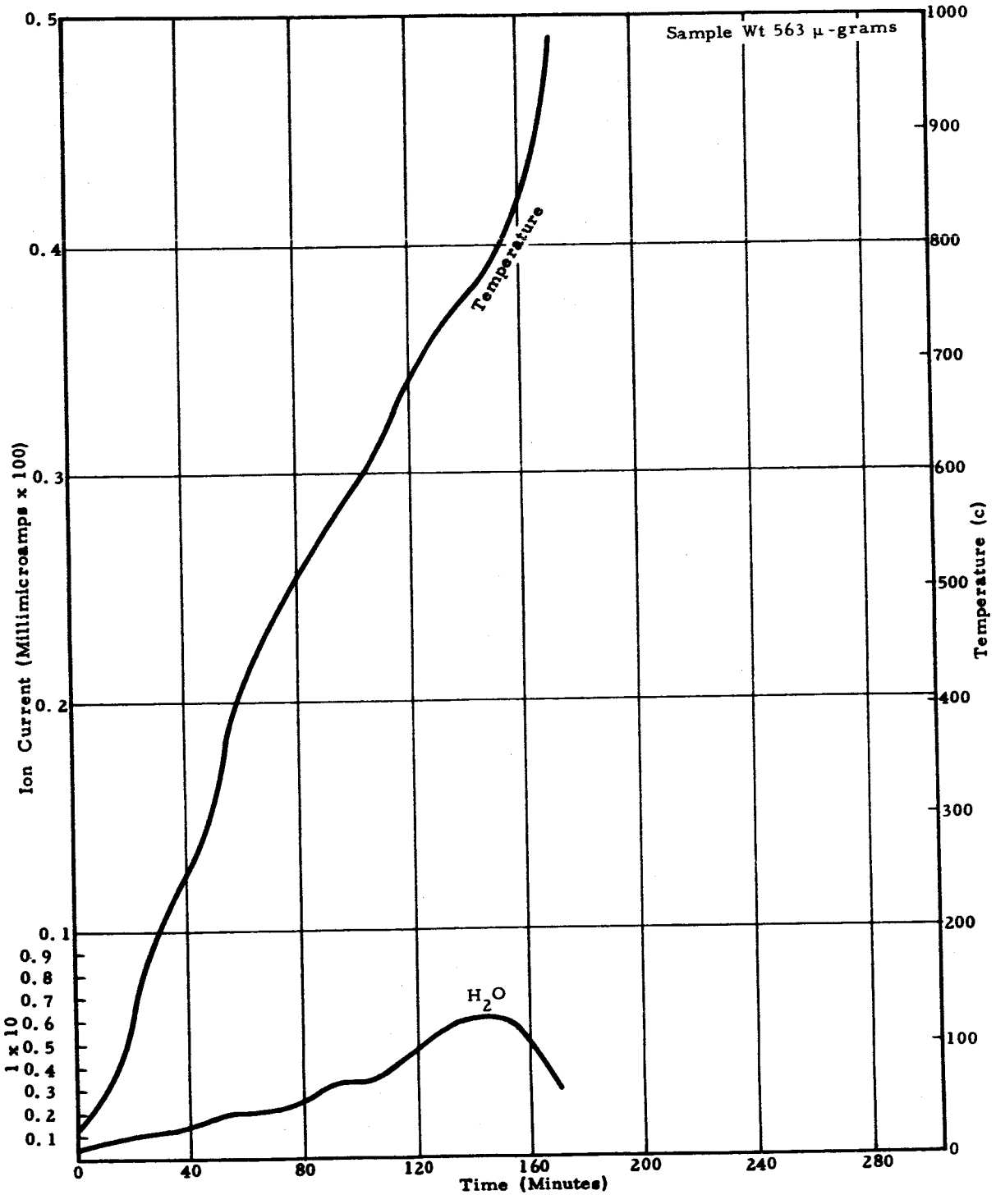

Figure 4-13 Mass Spectrometer Analysis of Hematite–Scan With H_20 Peak Plotted

4.10 MUSCOVITE

There are no compositional changes evident in the mass spectrometer curve (Figure 4-14) or the DTA curve. The TGA curve, however, indicates a 3% weight loss that can be attributed to absorbed water. Conversely, the mass spectrometer analysis reveals a water loss of < 1%. This discrepancy may be explained by the likelihood that water had been absorbed by the specimen during the grinding process, which was immediately removed upon subsequent exposure to vacuum in the mass spectrometer.

4.11 NATROLITE

Dehydration of the sample occurred at 40°C in the mass spectrometer. The curve (Figure 4-15) exhibits one sharp peak followed by a very low but continuous water loss. In contrast, the DTA curve indicates a large initial endothermic drift culminating in a sharp endothermic peak at 400°C. This endothermic drift results from the initial loss of water, either structural or absorbed. The water loss was not observed in the mass spectrometer, probably due to its immediate volatilization when placed under vacuum.

4.12 PLAGIOCLASE: IRRADIATED AND NONIRRADIATED

Analysis of the mass spectrometer curves discloses that neither the irradiated (Figure 4-16) nor the nonirradiated (Figure 4-17) specimens had undergone chemical change when subjected to a pressure of 5×10^{-6} torr and a range of temperatures up to 1000°C. However, a small loss of water, < 1%, is indicated in both cases. Confirmation of the absorbed water loss is evidenced by the slight endothermic drift of the DTA curves and the negative drift of the TGA curve.

4.13 TALC

The loss of a very small amount of absorbed water is indicated on the mass spectrometer curve (Figure 4-18) with the loss of OH^- taking place at 579°C. The DTA curve reflects this situation by showing a slight endothermic drift with an endothermic peak at 925°C.

4.14 TEKTITE

No changes are evident on the mass spectrometer curve (Figure 4-19), except for the loss of some absorbed water, estimated at < 1%. This analysis is confirmed by the slight endothermic drift of the DTA curve.

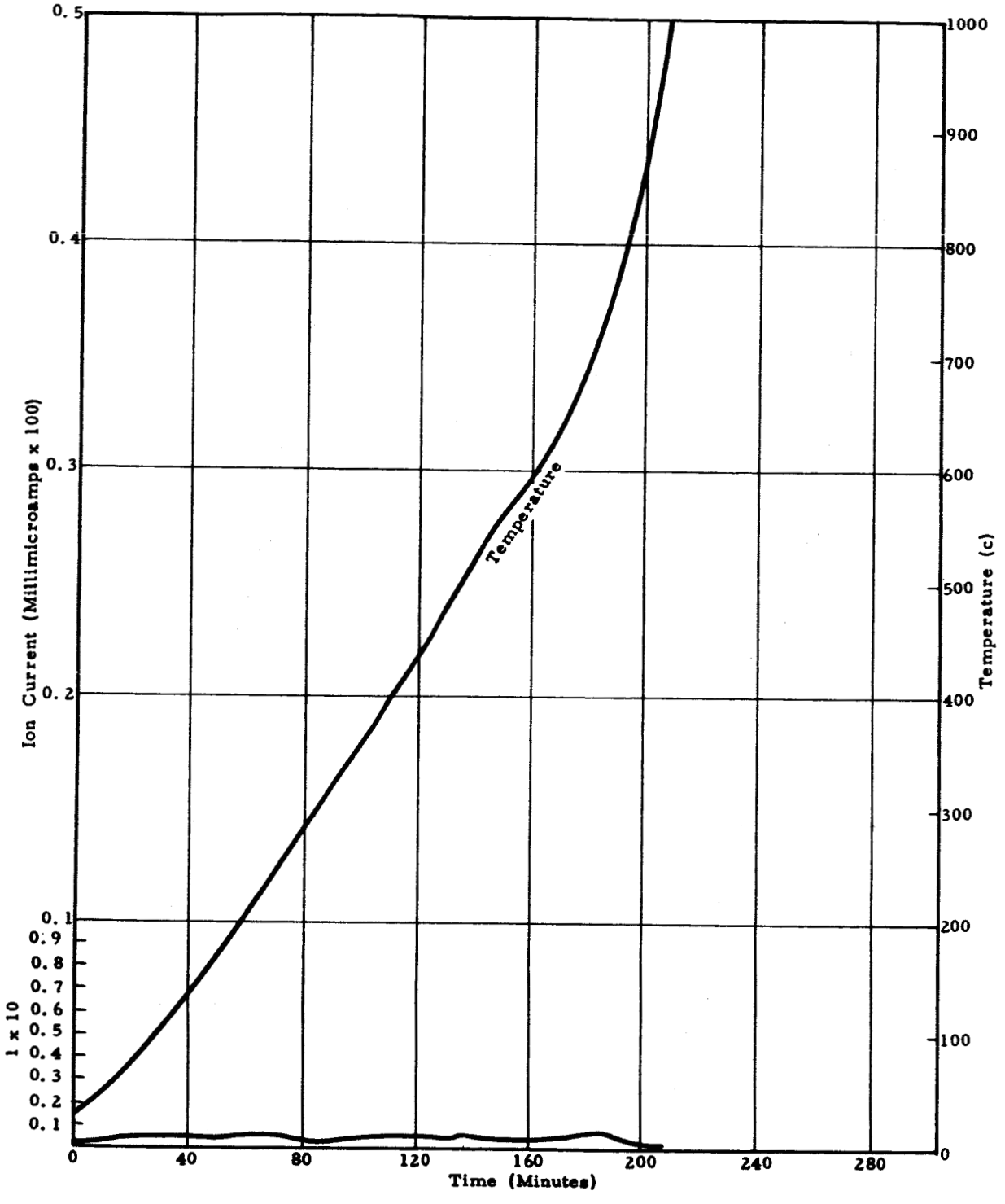

Figure 4-14 Mass Spectrometer Analysis of Muscovite-H_2O Peak

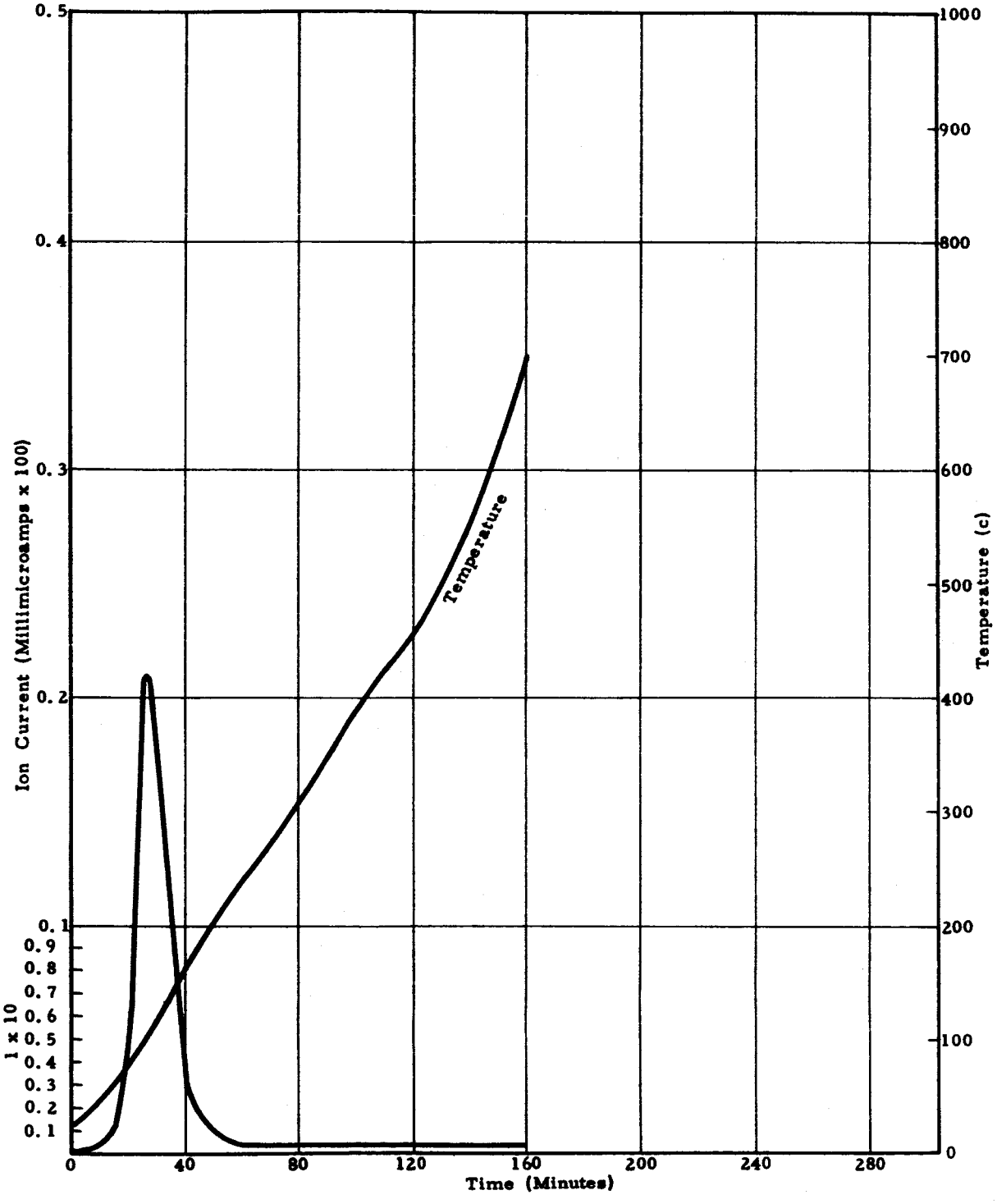

Figure 4-15 Mass Spectrometer Analysis of Natrolite–H_2O Peak

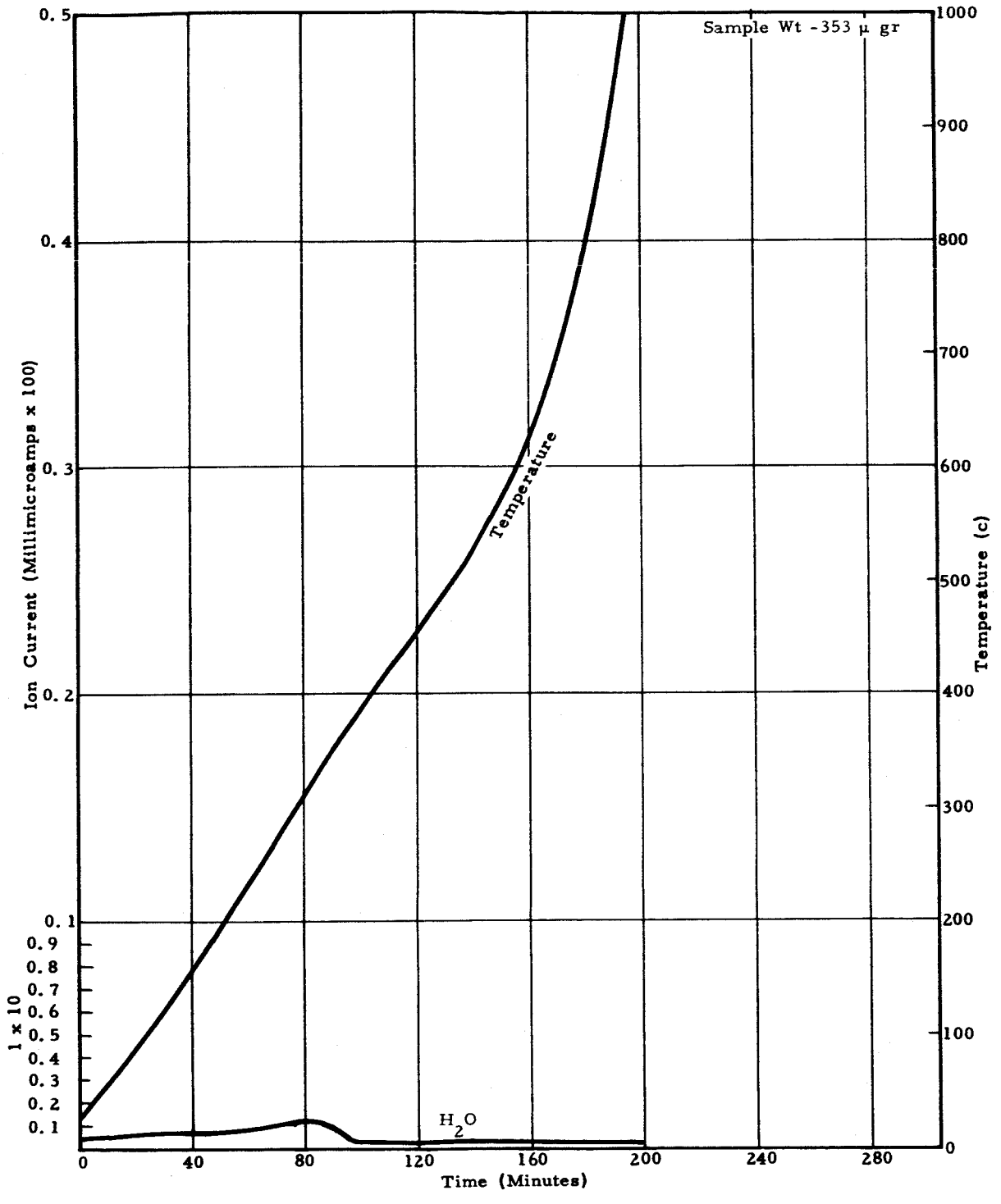

Figure 4-16 Mass Spectrometer Analysis of Plagioclase (Irradiated Labradorite)–H_2O Peak

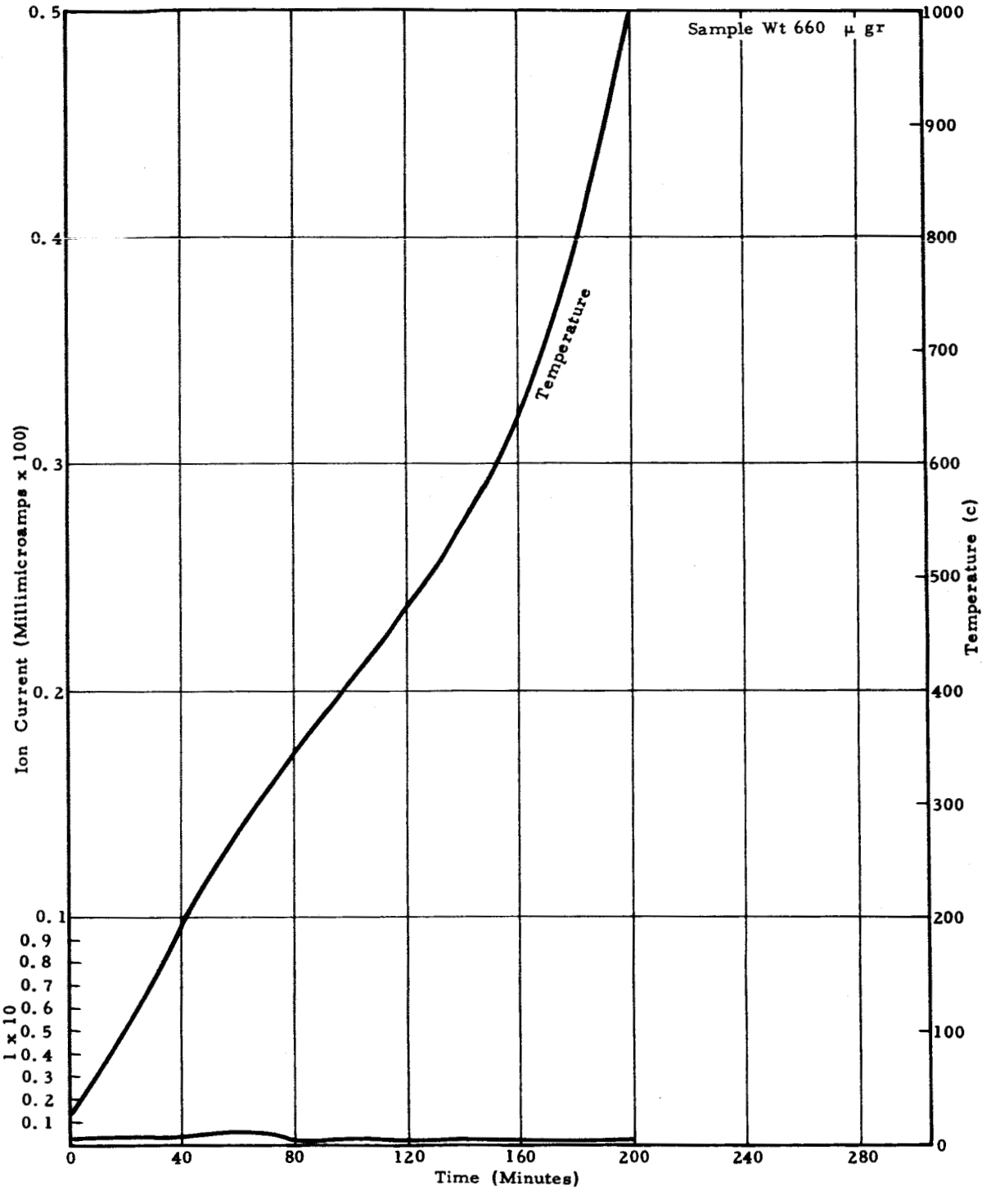

Figure 4-17 Mass Spectrometer Analysis of Plagioclase (Nonirradiated Labradorite–H_2O Peak

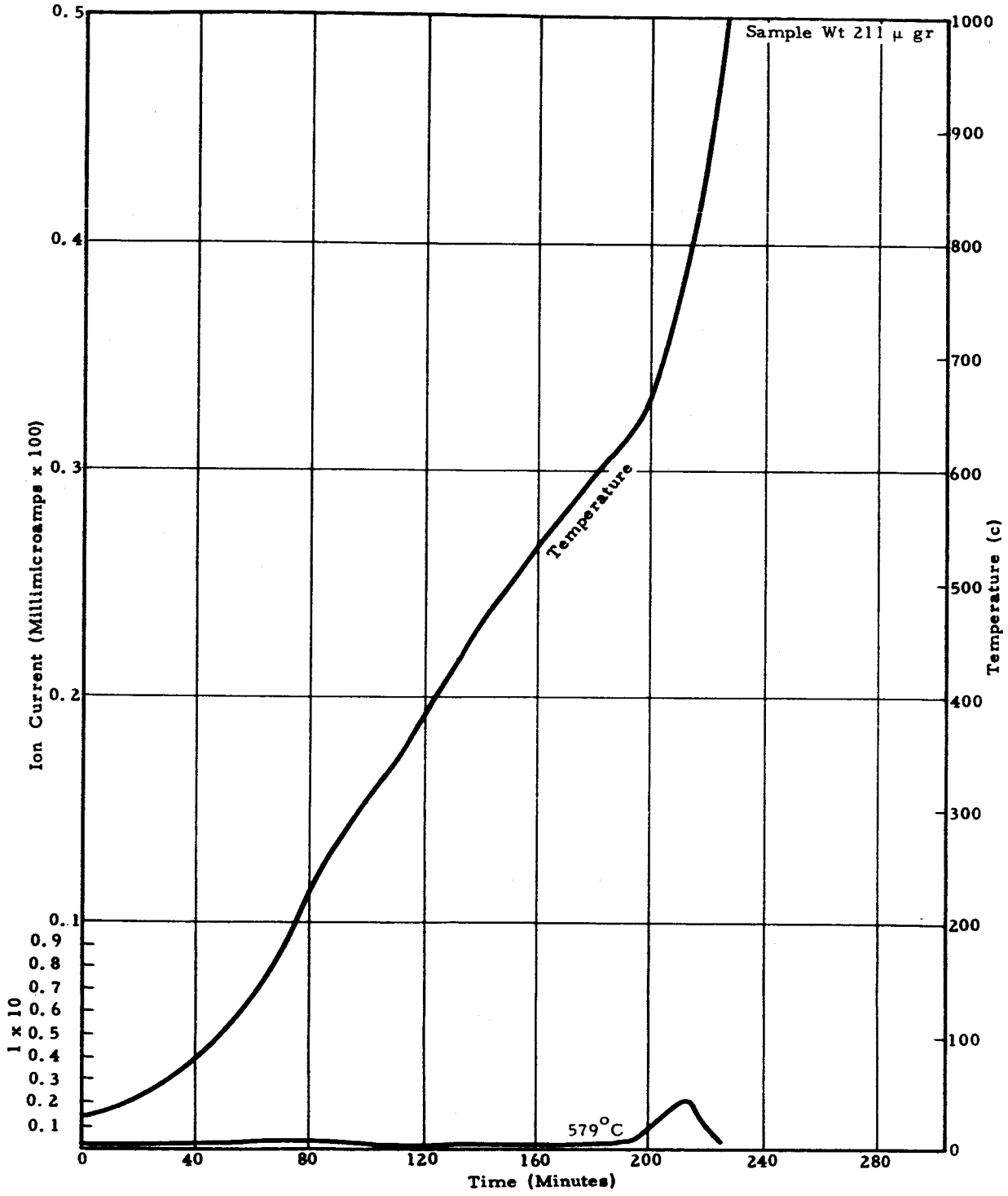

Figure 4-18 Mass Spectrometer Analysis Talc–H_2O Peak Plotted

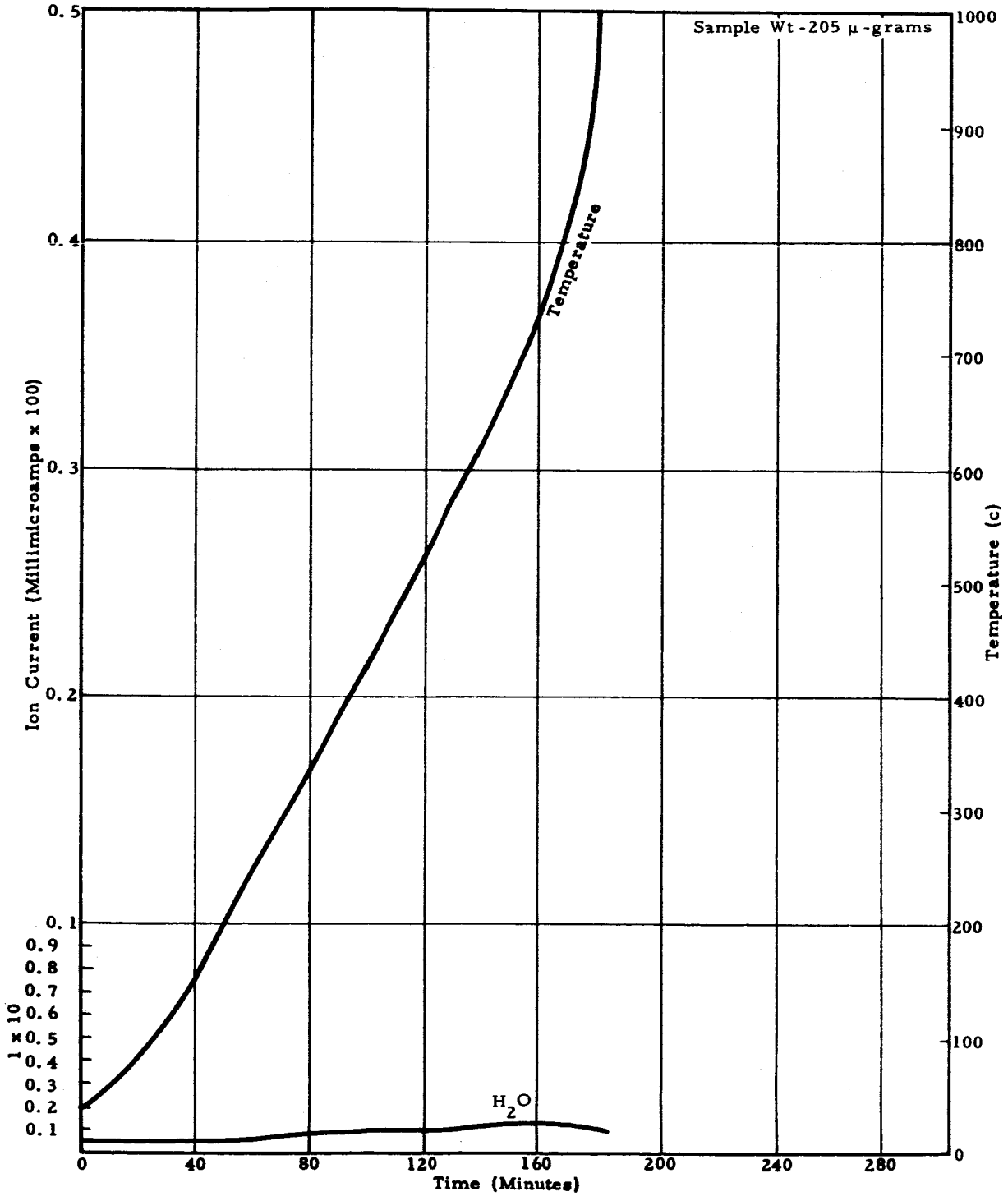

Figure 4-19 Mass Spectrometer Analysis of Tektite-H_2O Peak Plotted

4.15 SUMMARY

It is evident from the above comparisons of mass spectrometer curves with the DTA and TGA curves that the reaction temperatures are considerably lower in the vacuum of the mass spectrometer. This is expected since the stability of a substance is dependent on the partial pressures of its gaseous constituents. Table 4-1 compares the pressures and temperatures of reaction recorded in the mass spectrometer and DTA analyses of the 14 test minerals.

TABLE 4-1

REACTION TEMPERATURES IN THE MASS SPECTROMETER AND DTA

Mineral	Reaction	Mass Spectrometer*		DTA	
		Pressure H_2O in MM Hg	T°C	Pressure H_2O in MM Hg	T°C
Actinolite	$Ca(MgFe)_5Si_8O_{22}(OH)_2 \rightarrow MgSiO_3 + SiO_2$ + diopside + H_2O	5×10^{-6}	790	12.5	970
Ammonium Feldspar	$6\ NH_4AlSi_3O_8 \cdot 1/2\ H_2O \rightarrow 6\ NH_4AlSi_3O_8 + 3\ H_2O$	5×10^{-6}	30	12.5	370
	$6\ NH_4AlSi_3O_8 \rightarrow 6\ NH_3 + 3\ Al_2O_3 \cdot SiO_2 + 16\ SiO_2 + 3\ H_2O$	5×10^{-6}	52	12.5	498
Antigorite	$Mg_3Si_2O_5(OH)_4 \rightarrow Mg_3Si_2O_7$ (dehydrated antigorite) + H_2O	5×10^{-6}	270 ± 5	12.5	490
Basalt Glass	None	5×10^{-6}	–	5×10^{-6}	–
Calcite	$CaCO_3 \rightarrow CaO + CO_2$	1×10^{-9} (CO_2)	323 ● 5	10^{-2} (CO_2)	738
Ca-Montmorillonite	$(AlMg)_8(Si_4O_{10})_3(OH)_{10} \cdot 12\ H_2O \rightarrow (AlMg)_8(Si_4O_{10})_3(OH)_{10} + 12\ H_2O$	5×10^{-6}	–	12.5	49
	$(AlMg)_8(Si_4O_{10})_3(OH)_{10} \rightarrow$ mullite, spinel or, γalumina + H_2O	5×10^{-6}	240	12.5	573
Goethite	$2\ FeO(OH) \rightarrow Fe_2O_3 + H_2O$	5×10^{-6}	44	12.5	284
Gypsum	$CaSO_4 \cdot 2\ H_2O \rightarrow CaSO_4 \cdot 1/2 H_2O_\beta + 3/2\ H_2O$	5×10^{-6}	–	12.5	145
	$CaSO_4 \cdot 1/2\ H_2O_\beta \rightarrow CaSO_4 + 1/2\ H_2O$	5×10^{-6}	52	12.5	190
Hematite	None	5×10^{-6}	–	12.5	–
Muscovite	None	5×10^{-6}	–	12.5	–
Natrolite	$Na_2Al_2Si_3O_{10} \cdot 2\ H_2O \rightarrow Na_2Al_2Si_3O_{10} + 2\ H_2O$	5×10^{-6}	40	12.5	289
Plagioclase					
a. Non-Irradiated	None	5×10^{-6}	–	12.5	–
b. Irradiated	None	5×10^{-6}	–	12.5	–
Talc	$Mg_3Si_4O_{10}(OH_2) \rightarrow 3\ MgSiO_3 + SiO_2 + H_2O$	5×10^{-6}	579	12.5	835
Tektite	None	5×10^{-6}	–	5×10^{-6}	–

* H_2O partial pressures are based upon an extrapolation of the total peak height (millimicroamps) vs gauge pressure curve, taking into account the presence of a 10 fold pumping baffle.

SECTION 5

OPTICAL MICROSCOPIC INVESTIGATION

Microscopic analyses of source material (anorthoclase, basalt, and labradorite) and test minerals (except for ammonium feldspar and the irradiated plagioclase) were conducted during the second quarter. No thin sections were prepared for calcite, calcium montmorillonite, gypsum (selenite), and muscovite, since all but the montmorillonite are clear single crystals. The montmorillonite may be described as finely divided and unconsolidated material. Since thin section examination of these specimens would provide no useful information, temporary grain mounts were made instead for refractive index determinations of these and certain other minerals.

Thin sections of the following specimens were studied under the optical microscope:

1. Actinolite
2. Anorthoclase - used for synthesis of NH_4 feldspar
3. Antigorite
4. Basalt - used for fusing basalt glass
5. Basalt glass
6. Goethite
7. Hematite
8. Labradorite - used for irradiation of plagioclase
9. Natrolite
10. Talc
11. Tektite.

Photomicrographs are herein included as reference. The refractive indices reported below are for sodium light and accurate to ±0.002. If any had been taken between crossed polars, a statement to that effect is made. Otherwise no mention is made of the light used.

5.1 ACTINOLITE

The thin section (Figure 5-1) shows that the material is very pure. It is estimated that about 1% of nearly colorless chlorite is present, with a minute amount of finely divided magnetite associated with the actinolite.

The actinolite appears pale green and has a maximum birefringence of 0.025, extinction angle $c \wedge \gamma = 17^{\circ}$, and negative optic sign, $2V = 85^{\circ}$.

5.2 ANORTHOCLASE

The anorthoclase is in part very clear (Figure 5-2). It does contain other phases which can not readily be removed. About 10% of iron oxide stained clay surrounds 1- to 2-mm ellipsoidal cavities. These cavities are lined with clear trapezohedrons of analcite. (Index of refraction is 1.485). There are a few black equidimensional black crystals. These crystals could not be identified by optical means.

The axial angle of the anorthoclase measures rather low, a little under 40°. The material is optically positive with $\alpha = 1.533$ and $\gamma = 1.54$. Some very fine lamellar twinning with nearly parallel extinction occurs in the crushed fragments of the feldspar.

5.3 ANTIGORITE

About half of the specimen in the thin section (Figure 5-3) is composed of veinlets of chrysotile a few millimeters wide. The cross fibers show high birefringence, parallel extinction, and are length slow. This chrysotile was easily separated from the host antigorite after the material had been coarsely crushed.

The antigorite appears very pale green, with low relief in Canada balsam. It is length fast, optically negative, with 2V about 20°. Aside from a minute amount of opaque magnetite, the easily separated antigorite is of high purity.

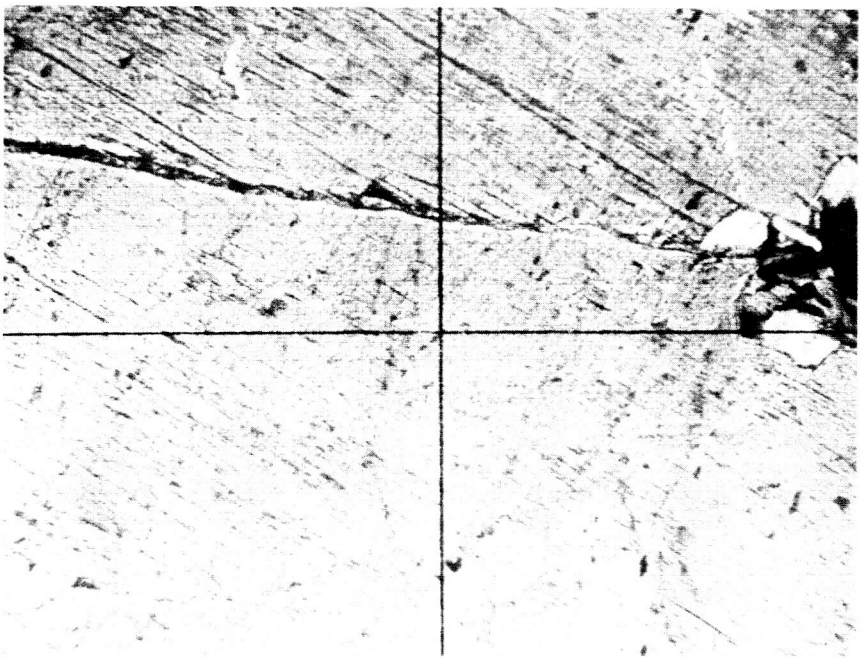

Figure 5-1 Photomicrograph of Actinolite, Crossed Polars, 47X, Chlorite Crystals at Right Edge

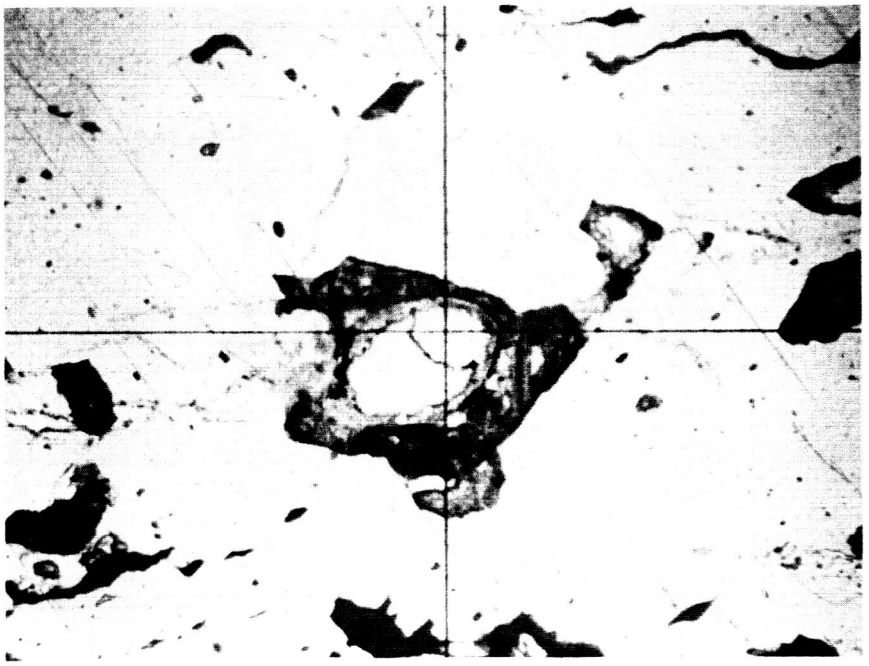

Figure 5-2 Photomicrograph of Anothoclase, 47X, Analcite Crystal at Center

Figure 5-3 Photomicrograph of Antigorite, Crossed Polars, 47X, Veinlet of Chrysotile in Upper Right Quadrent

Figure 5-4 Photomicrograph of Basalt, Crossed Polars, 47X

5.4 BASALT

The basalt is very clean looking (Figure 5-4). The composition, as determined from one thin section of the uniform sample, consists of:

Labradorite laths to 0.4-mm long	50%
Labradorite zoned phenocrysts, 1 mm	5%
Pigeonite (2 V = 30°, optically positive, birefringence about 0.025). Grains 0.05 to 0.2 mm	30%
Opaque groundmass, devitrified glass	10%
Serpentine, yellow stained after olivine	5%

5.5 BASALT GLASS

The fusing of the basalt produced a brown scoriaceous glass with many gas bubbles (Figure 5-5). About 2% of fine crystallites gives the glass a cloudy appearance. These are no doubt a result of devitrification during cooling. About 6% of unmelted labradorite crystals, (relics of the larger phenocrysts), are scattered throughout the glass. The index of refraction of the glass is 1.595.

5.6 CALCITE

The clear calcite is of high purity. No other phases were seen under the microscope (Figure 5-6). The glide twinning characteristic of crushed calcite was quite evident in the grains studied. The ordinary index of refraction is 1.658.

5.7 CALCIUM MONTMORILLONITE

The material is finely divided (Figure 5-7). The largest grains do not exceed 2 μ in diameter. The only impurity observed was a few minute quartz grains. The γ index of the calcium montmorillonite is 1.505.

5.8 GOETHITE

The deep brown-red color, the colloform structure, and parallel extinction are typical of goethite. Some portions of the thin section (Figure 5-8)

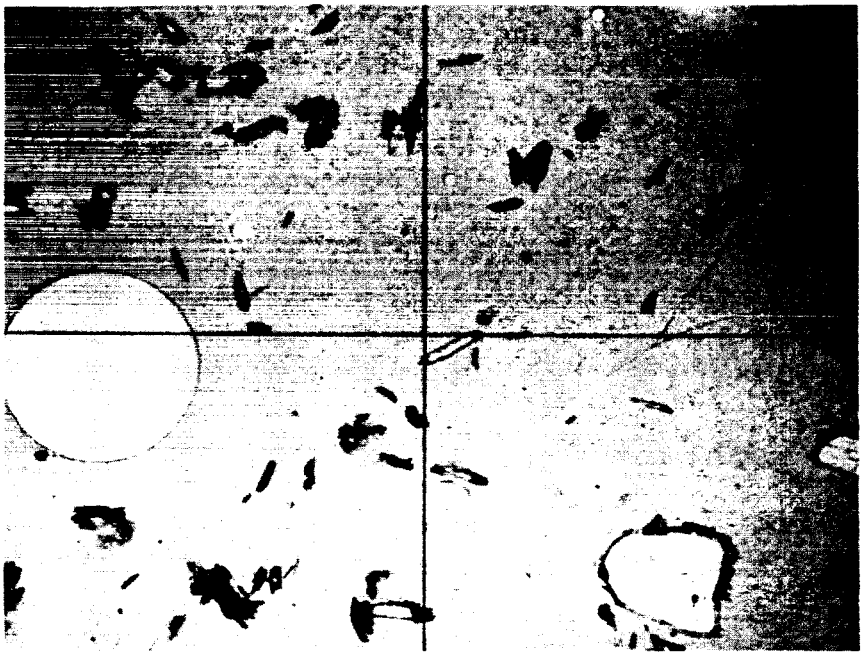

Figure 5-5 Photomicrograph of Basalt Glass, 47X, Gas Bubble at Left Plagioclase Relic at Lower Right, Crystallites Scattered Over Field

Figure 5-6 Photomicrograph of Calcite, 210X, The DTA Sample in Medium Having Index of Refraction of 1.56

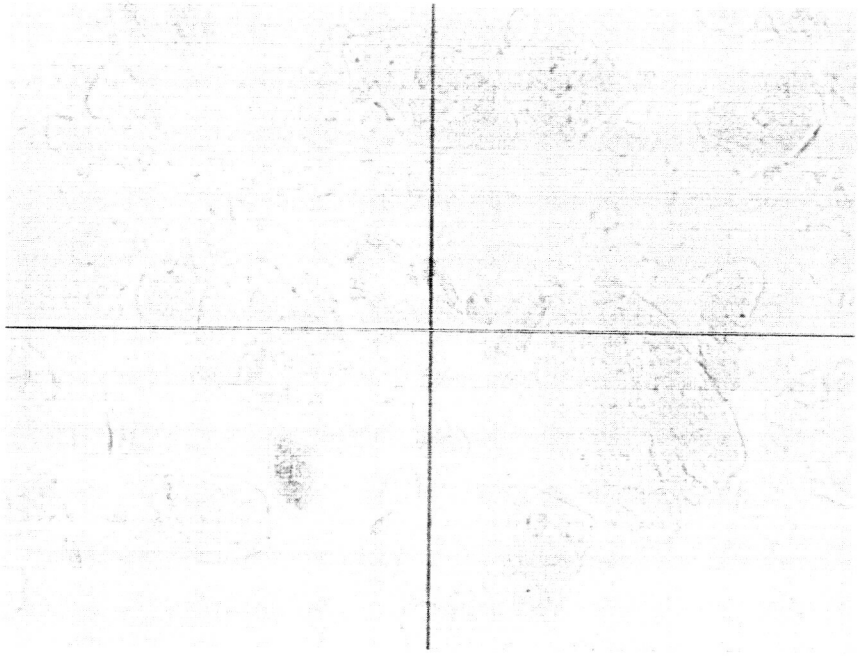

Figure 5-7 Photomicrograph of Ca-Montomorillonite, 210X, The Untreated Sample in Medium Having Index of Refraction of 1.48

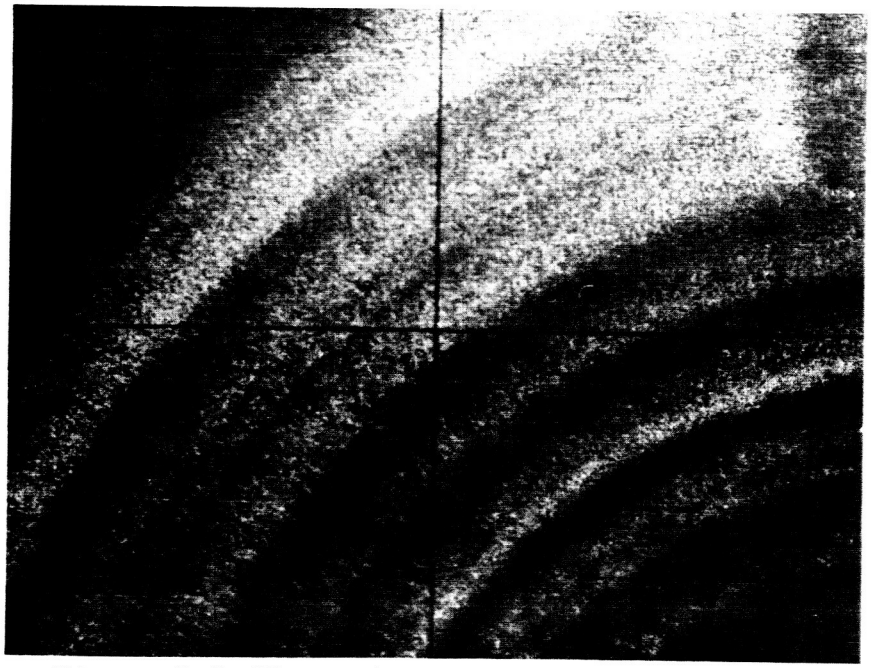

Figure 5-8 Photomicrograph of Goethite, 47X

appear opaque, probably because of the perpendicular orientation of the fibers with respect to the plane of the section. No impurities were seen in the microscopic examination.

5.9 GYPSUM

The clear selenite cleavage flakes show a centered flash interference figure (Figure 5-9). The α index is 1.520. No impurities are visible under the microscope.

5.10 HEMATITE

The hematite (needle ore) is too opaque for conventional microscopic analysis. Only the thinnest edges show a deep red color in transmitted light. In reflected light, the material appears steel gray to red. Under the binocular microscope there are no visible impurities in the dense fibrous mass (Figure 5-10).

5.11 LABRADORITE

The labradorite is very coarsely crystalline. Albite twinning is a prominent feature, with pericline twinning present to a lesser degree. Although some cracked areas have been altered to white opaque kaolin, the material in the slide (Figure 5-11) appears clear and fresh. About 0.5% pyroxene (augite or diopside) occurs in small clusters of crystals. Some of these crystals range as large as 0.2 mm in diameter. A minor amount (a very small fraction of 1%) of dark brown to black needles lie parallel to the (010) plane. A few are randomly oriented. They measure up to several tenths of a mm long and from 1 to 10 μ in diameter, and can almost certainly be identified as rutile.

With the slide on the universal stage and employing the Rittmann zone method, it was possible to determine the composition of the labradorite as $Ab_{48}An_{52}$. The extinction angles, however, measured on (010) and (001), showed an identical composition. However, the indices of refraction determined on crushed fragments ($\alpha' = 1.558$) indicate a somewhat more calcic composition.

5.12 MUSCOVITE

The clear cleavage fragments contain a small fraction of 1% of tiny opaque specks, probably magnetite (Figure 5-12). The muscovite is optically negative, has a 2 V of about 40°, and the indices $\beta = \gamma = 1.590$.

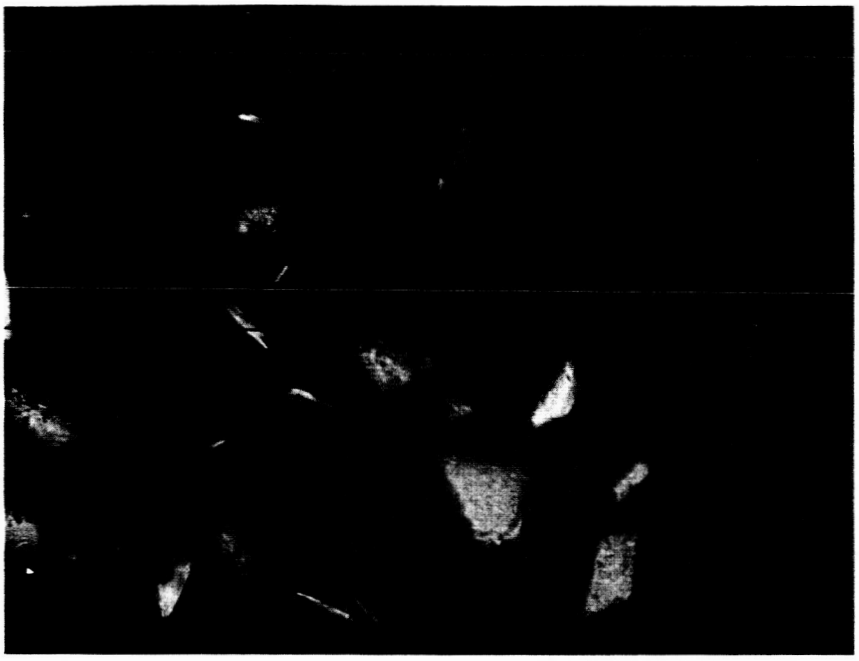

Figure 5-9 Photomicrograph of Gypsum, Crossed Polars, 210X, The DTA Sample in Liquid Having Index of Refraction of 1.56

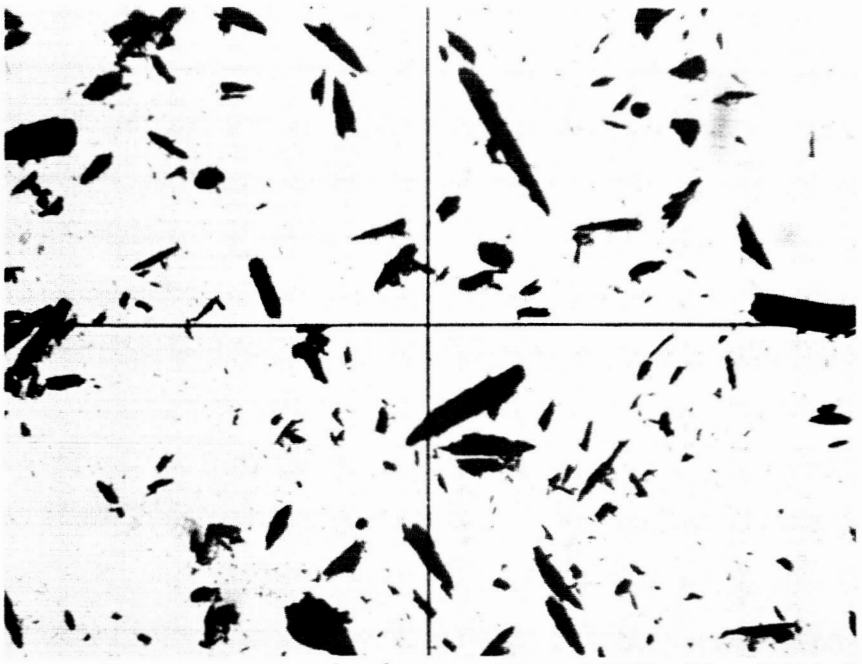

Figure 5-10 Photomicrograph of Hematite, 100X, The DTA Sample in Liquid Having Index of Refraction of 1.68

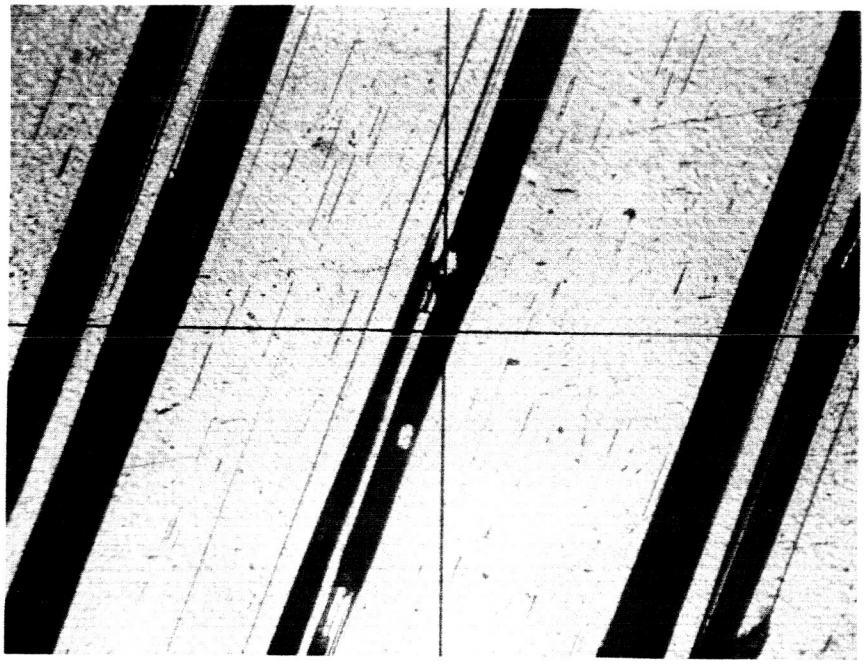

Figure 5-11 Photomicrograph of Labradorite, Crossed Polars, 47X, Shows Albite Twinning, Rutile Needles (Parallel With Twinning), and Pyroxene Crystals in Central Dark Twin Band

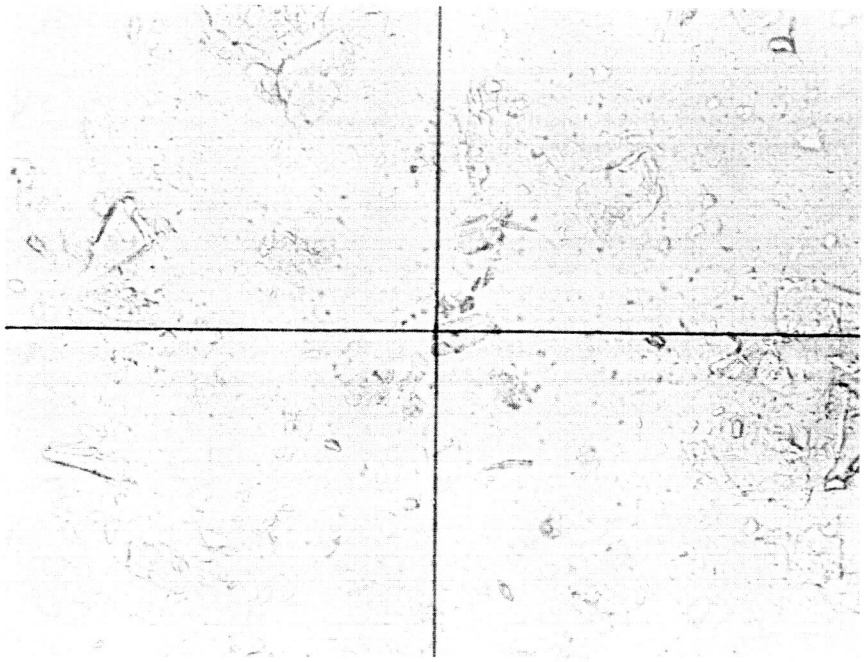

Figure 5-12 Photomicrograph of Muscovite, 210X, DTA Sample Immersed in Liquid Having Index of Refraction of 1.48

5.13 NATROLITE

The natrolite was received from Wards in two separate shipments, with certification that both originated from the same locality. The first consists of radial aggregates of coarse cream-colored and somewhat rusty looking natrolite attached to an altered porphyritic basic rock. The practically square prisms are length slow. $\gamma = 1.490$. The amount of iron oxide stain is negligible.

The second batch of natrolite specimens is similar in nature, but without rust stain. The crystals appear snow white. A large amount of the closely related zeolite, scolecite, is intermixed with the coarse natrolite. The scolecite occurs in fine fibers and is length fast. The angle $\alpha \wedge c = 18^{\circ}$. It should be noted that the thin section (Figure 5-13) includes a sample from the second batch. Although both batches contained a large amount of analcite, it was readily separated from the natrolite and scolecite for the experiments.

5.14 TALC

The talc, occurring as clear foliated masses, does not contain tremolite, chlorite, or carbonates in the thin section. However, a fraction of one percent of black opaque material, probably magnetite, is present. The talc is optically negative, colorless in thin sections (Figure 5-14), shows low relief in Canada balsam, and has a measured axial angle of zero.

5.15 TEKTITE

The tektite appears quite homogeneous except for some small blocky optically isotropic inclusions which are probably lechatlierite (silica glass). (Figure 5-15) Also, a few dust-like particles are scattered throughout the glass of the tektite. The index of refraction of the tektite glass measures 1.495. The mass of the specimen does not show flow structure.

5.16 SUMMARY

Optical microscopic examination of 12 of the 14 test minerals has been completed to date. As soon as another batch of ammonium feldspar is produced, it will be checked out along with the irradiated feldspar.

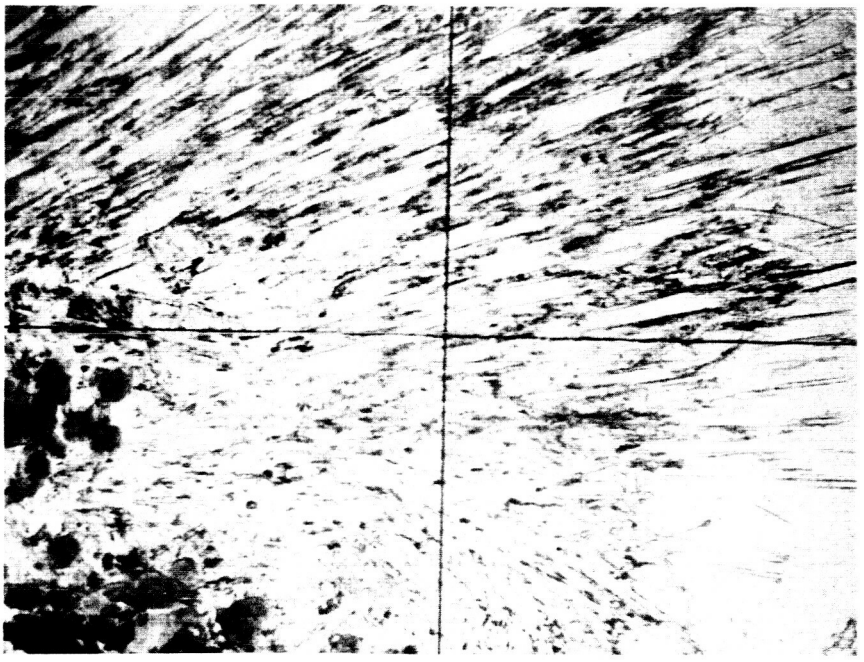

Figure 5-13 Photomicrograph of Natrolite, 47X, Coarse Needles of Natrolite and Fine Needles of Scolecite in Central Area, Analcite in Clear Right Area, Wall Rock in Lower Left Quadrant

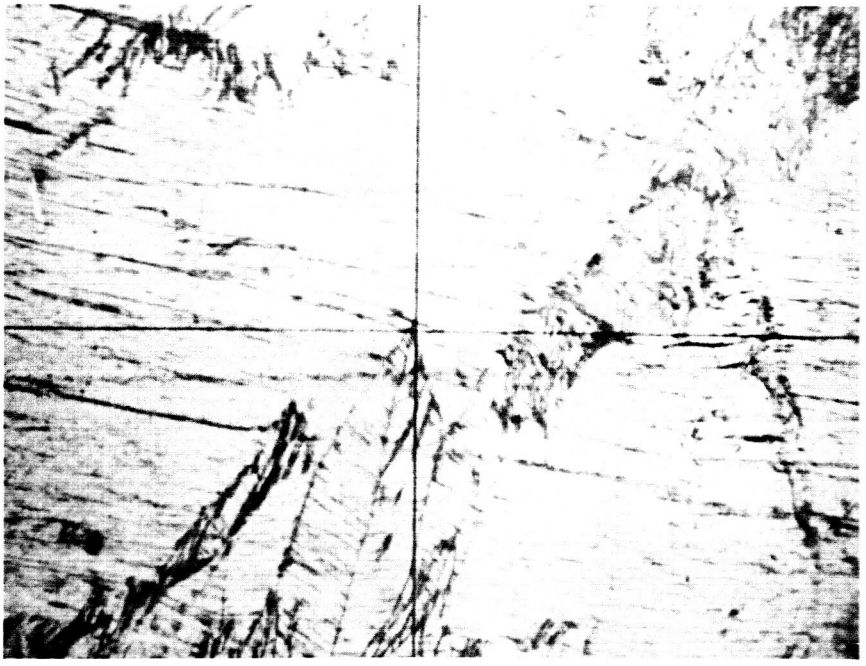

Figure 5-14 Photomicrograph of Talc, 47X

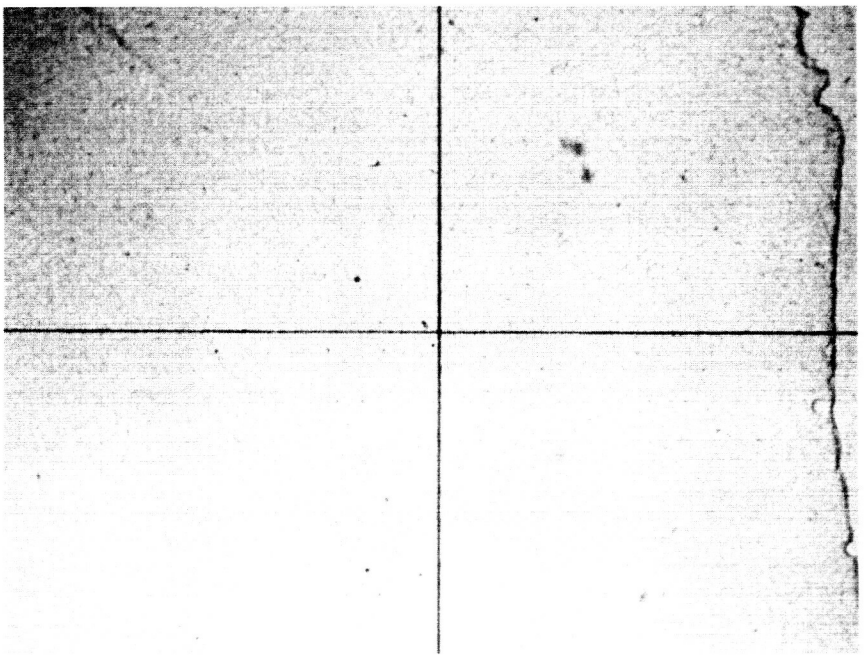

Figure 5-15 Photomicrograph of Tektite, 47X

SECTION 6

FABRICATION OF LONG-TERM TEST APPARATUS

6.1 CHECKOUT OF ULTRAHIGH VACUUM SYSTEM

The ultrahigh vacuum system (Figure 6-1) was assembled and tested for ultimate vacuum capability. When vacuum of only 1×10^{-9} torr was achieved, it was decided to return the unit to the manufacturer for repairs.

At Varian Associates, California, the chamber was evacuated, baked, leak-tested by helium mass spectrometer, and pumped to ultimate. The empty chamber pressure dropped from 3×10^{-7} to 4.4×10^{-11} torr in an 8-hour period. Since one of the reasons for the poor performance had been a too low bakeout, it was subsequently discovered that the original instruction manual discribing the procedures for sequencing the titanium pumps, the ultimate bakeout temperature, and the temperature rating of the ion pump magnets, was in error. When the unit was returned to Bendix, the correct manual accompanied the shipment.

6.2 X-RAY CAMERA-BRAZING THE BERYLLIUM WINDOW

The brazing of the x-ray window posed an extremely difficult problem in the fabrication of the X-ray camera. It required that the beryllium strip be bonded to the stainless steel housing, with absolutely no leak detectable using the most sensitive helium mass spectrometer. The braze line is roughly 22-in. long, much longer than any similar braze having the same vacuum requirements. Basically, the process of brazing beryllium to stainless steel consists of a rigorous chemical cleaning of the surface, preplating with refractory metals (gold, platinum, etc), and heating the parts under vacuum. The brazing material, a special alloy of silver, is held as a sandwich filler between the base materials. The actual process may vary in some details, as they are trade secrets.

Several vendors, who regularly do this type of brazing, were contacted. The first one selected, on the basis of price and performance claims, failed to make a leak-proof braze. The camera was next sent to the Brush

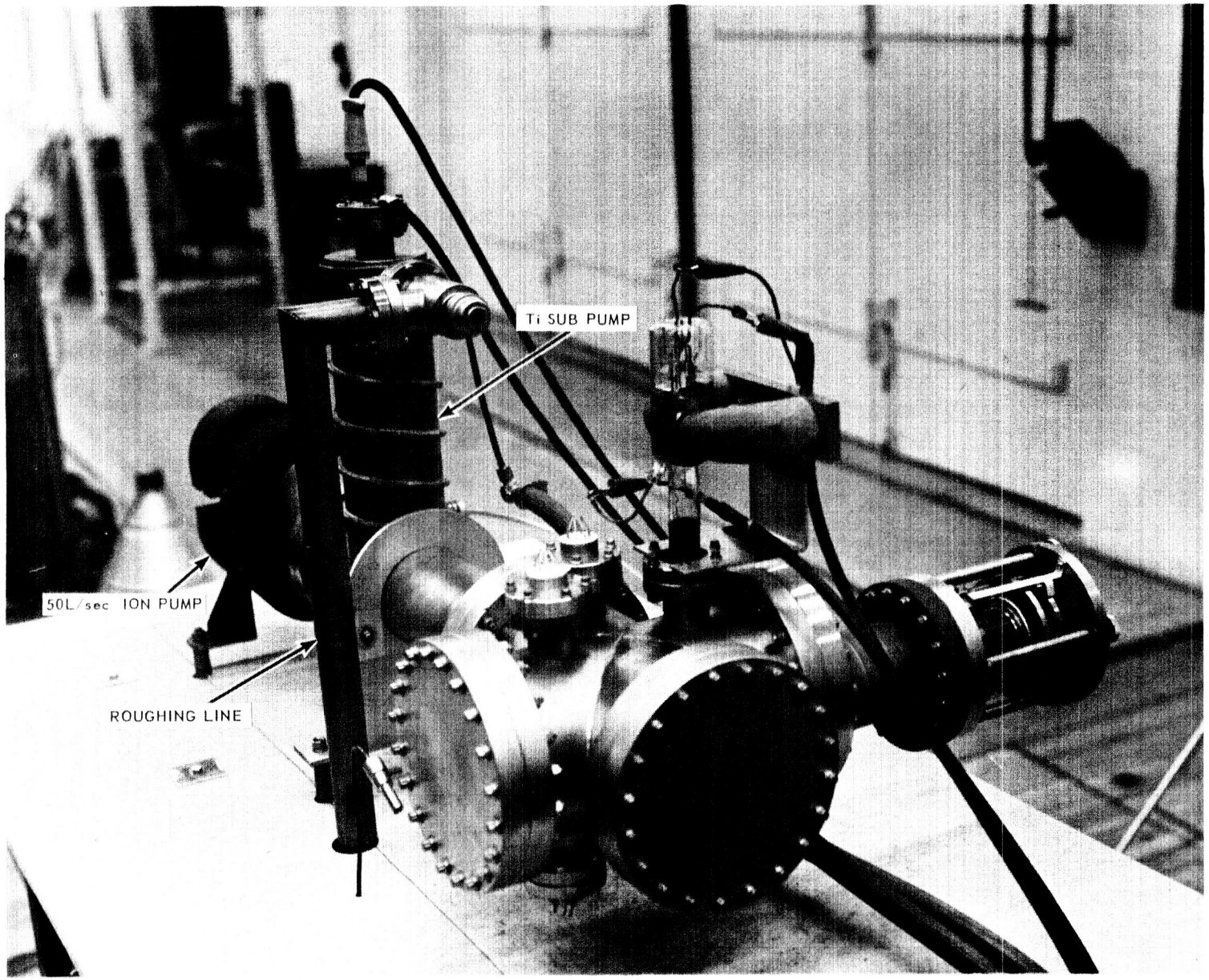

Figure 6-1 Ultrahigh Vacuum System for Long Term Experiment

Beryllium Laboratory in Cleveland, where they attempted to braze the beryllium window. After failing the first time, Brush Beryllium recommended a modification to the camera which Bendix accepted. It was suggested that a flat be removed from the braze area. This had caused a problem in holding a proper pressure between the base materials. The flat was removed and the braze was succesfully accomplished and proved leak-tight. No discernible leak could be detected on the helium mass spectrometer.

The camera (Figure 6-2) was then checked for alignment and secondary X-ray emission. These tests showed that the fixture was properly aligned and, while not certain, the secondary emission from the stainless steel did not appear to affect the diffraction patterns.

6.3 X-RAY SAMPLE HOLDER

After assembling the whole fixture (Figure 6-3) and calibrating the positioning device, it was discovered that the sample holders would not traverse the beam in a straight line. The trouble was traced to eccentricity in the lead screw, which was amplified in the cantilevered construction of the sample holder. A new design had to be formulated to eliminate this problem. It consists of an extension shaft, a ball bearing, and an eccentric adjustment. The new feature has been fabricated and successfully tested, reducing the eccentricity of the boat holder to 0.015 in. which is well within the X-ray beam width of 0.031 in. The long term test apparatus is now ready for operation (Figure 6-4).

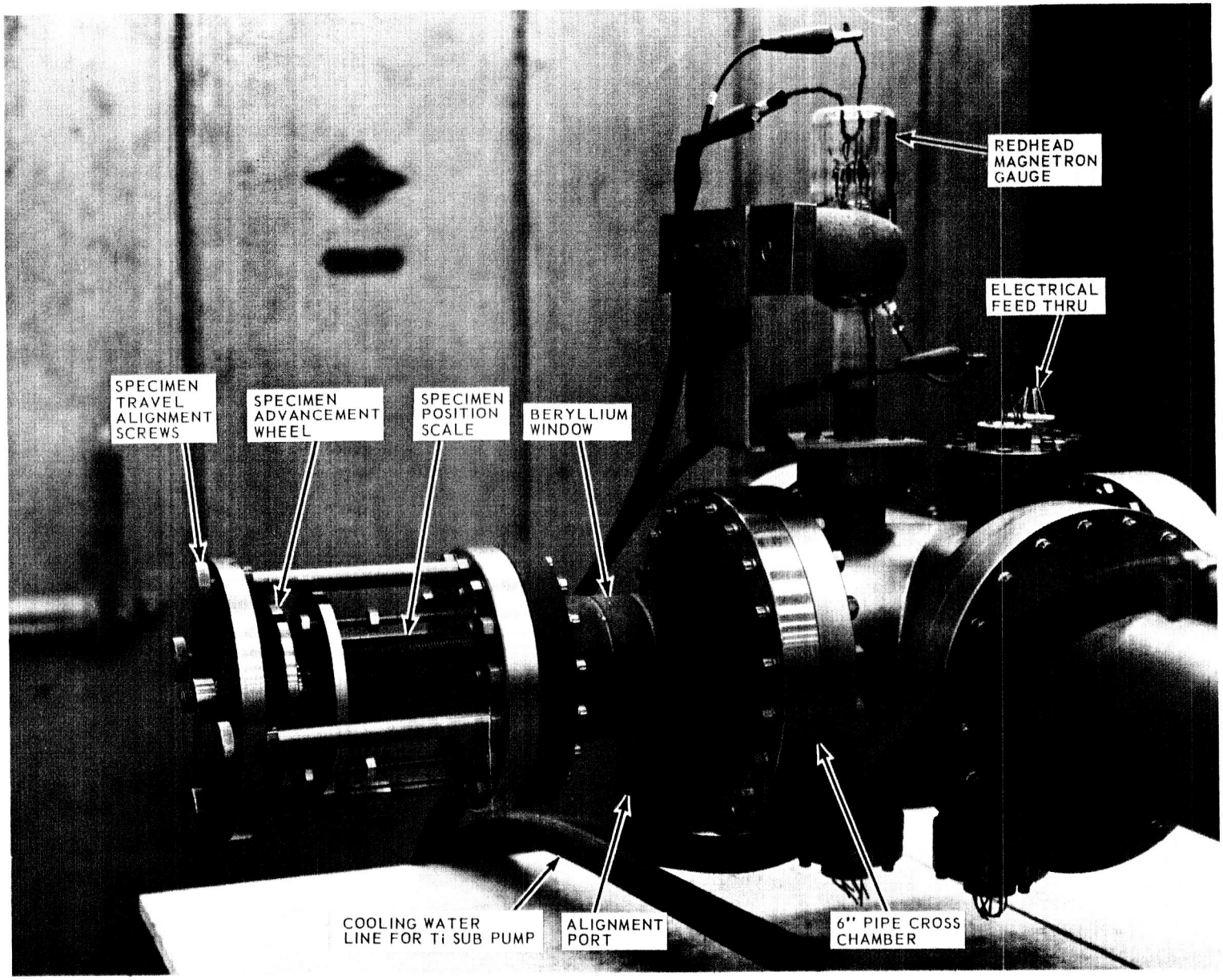

Figure 6-2 X-Ray Camera Unit Attached to Ultrahigh Vacuum System

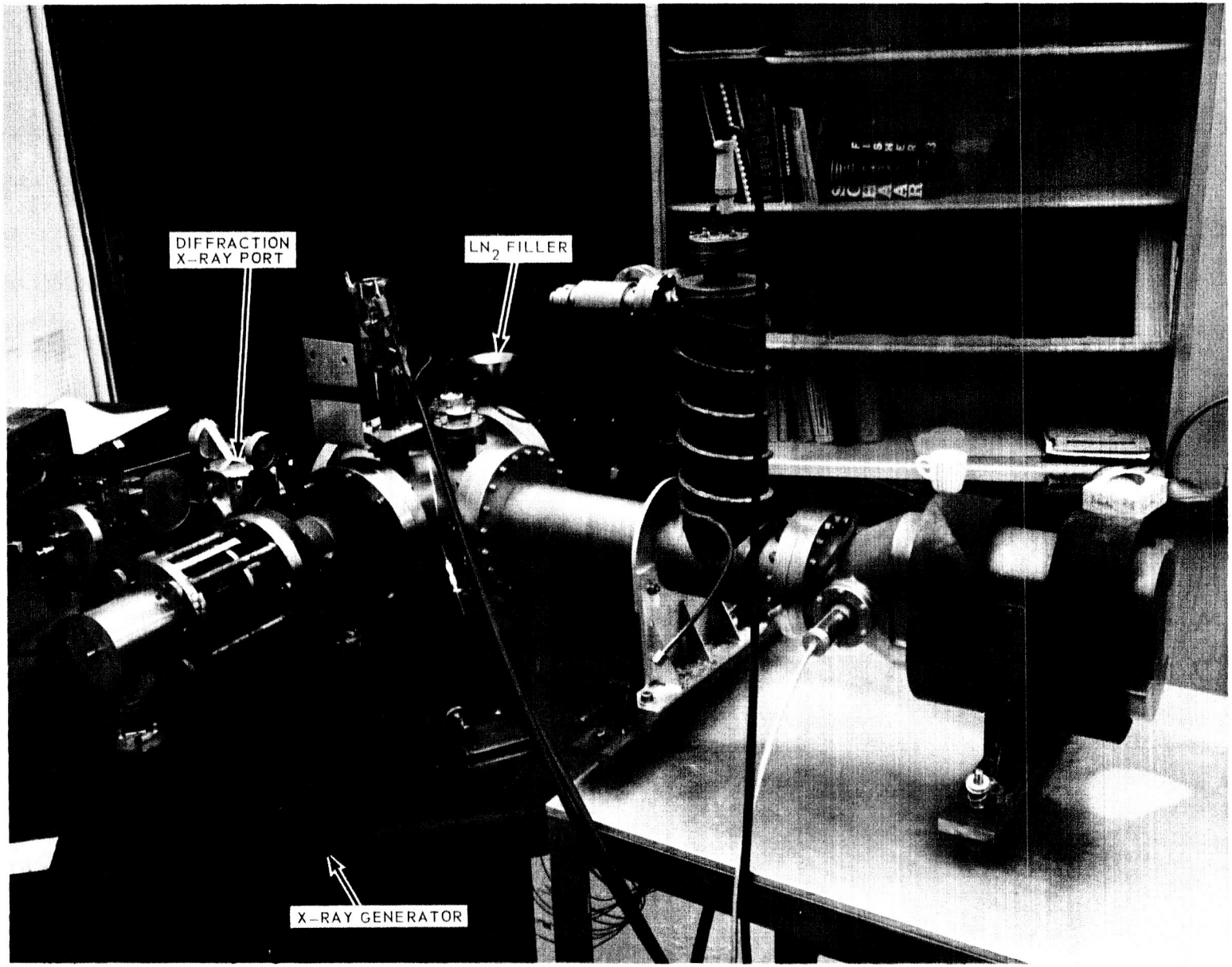

Figure 6-3 Long Term Test Apparatus Completely Assembled

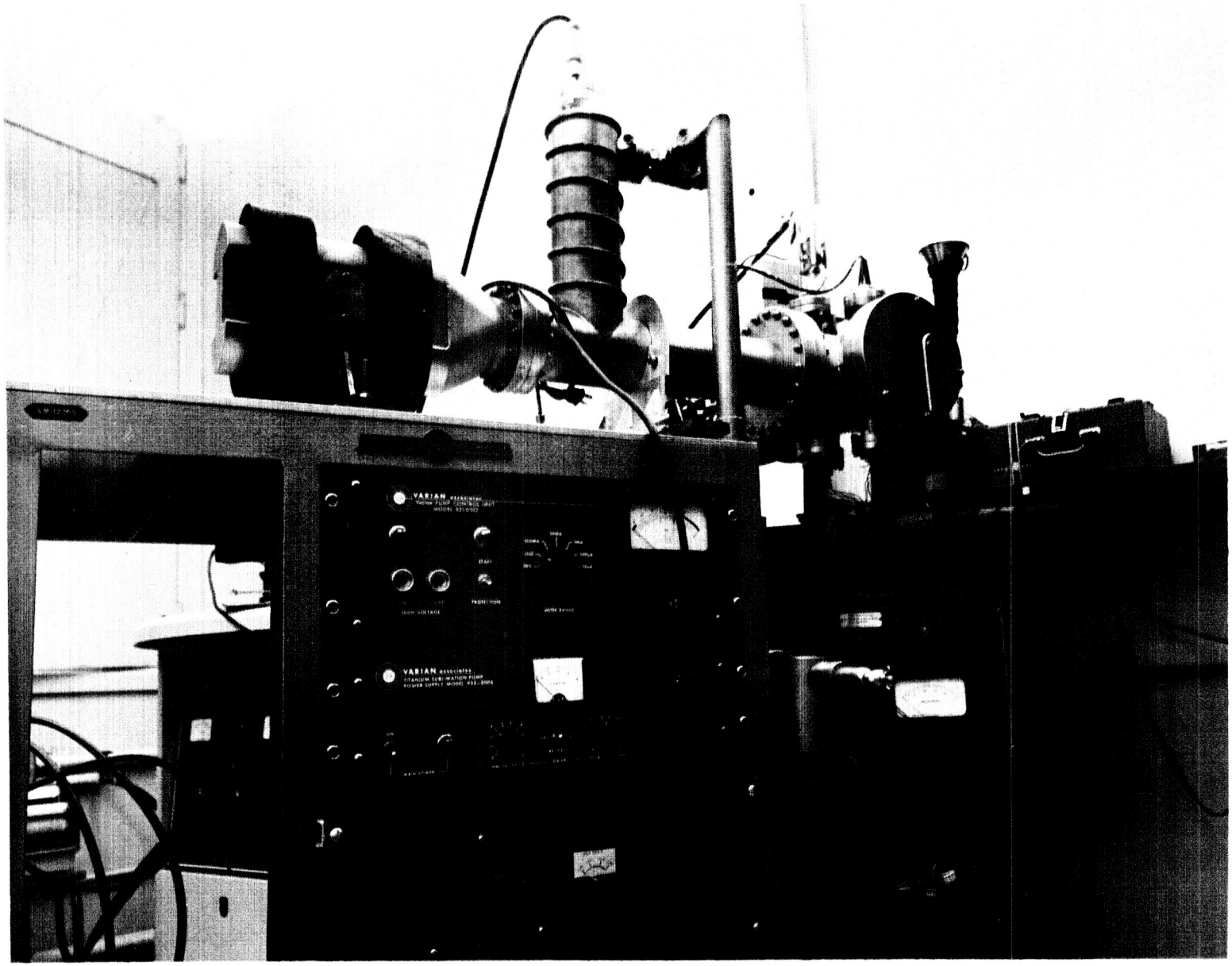

Figure 6-4 Long Term Test Apparatus—View Showing Control Panels on Vacuum System and X-Ray Generator

SECTION 7

PLANNED RESEARCH FOR THE THIRD QUARTER

The work to be carried out in the next quarter will follow closely that outlined in Bendix's Technical Proposal, BSD 965. The tasks to be performed in the third quarter are described below:

1. Complete the preparation of 135 gm of ammonium feldspar and forward 100 gm together with 100 gm of irradiated plagioclase to NASA-MSC.

2. Accomplish the short term experiment in two stages. First, standard patterns of the 14 minerals will be obtained under room temperature and atmospheric pressure conditions in the X-ray camera to be used for the long term experiment. These photographs will be used for comparison purposes in the long term experiment. Second, those minerals for which reactions and transformations are most likely to occur under the long term conditions will be X-rayed individually in the ultrahigh vacuum chamber at temperatures high enough to assure that transformation had taken place. These will also serve as standard photographs for the long term experiment and, in addition, will be used to verify the results of the mass spectrometer analyses.

3. Fabricate sample holder for vacuum chamber, which will store samples for chemical analysis.

4. Initiate the long term experiment at the conclusion of the short term experiment.